
TEFL: Prediction-Residual-Guided Rolling Forecasting for Multi-Horizon Time Series

Xiannan Huang¹ Shen Fang² Shuhan Qiu¹ Chengcheng Yu¹ Jiayuan Du³ Chao Yang¹

Abstract

Time series forecasting plays a critical role in domains such as transportation, energy, and meteorology. Despite their success, modern deep forecasting models are typically trained to minimize point-wise prediction loss without leveraging the rich information contained in past prediction residuals from rolling forecasts—residuals that reflect persistent biases, unmodeled patterns, or evolving dynamics. We propose **TEFL** (Temporal Error Feedback Learning), a unified learning framework that explicitly incorporates these historical residuals into the forecasting pipeline during both training and evaluation. To make this practical in deep multi-step settings, we address three key challenges: (1) selecting observable multi-step residuals under the partial observability of rolling forecasts, (2) integrating them through a lightweight low-rank adapter to preserve efficiency and prevent overfitting, and (3) designing a two-stage training procedure that jointly optimizes the base forecaster and error module. Extensive experiments across 10 real-world datasets and 5 backbone architectures show that TEFL consistently improves accuracy, reducing MAE by 5–10% on average. Moreover, it demonstrates strong robustness under abrupt changes and distribution shifts, with error reductions exceeding 10% (up to 19.5%) in challenging scenarios. By embedding residual-based feedback directly into the learning process, TEFL offers a simple, general, and effective enhancement to modern deep forecasting systems.

*Equal contribution ¹Key Laboratory of Road and Traffic Engineering, Ministry of Education Tongji University, Shanghai China ²Research Center for Scientific Data Hub, Zhejiang Lab, Hangzhou, China ³The College of Computer Science, Tongji University, Shanghai China. Correspondence to: Chao Yang <tongjiyc@tongji.edu.cn>.

1. Introduction

Time series forecasting is of great significance in many fields such as finance, transportation, healthcare, meteorology, and energy (Gruca et al., 2023; Kadiyala & Kumar, 2014; Morid et al., 2023). In recent years, deep neural networks have become dominant in this domain (Liu et al., 2023; Zhou et al., 2021). These models are typically trained on randomly sampled consecutive segments: the past segment serves as input, and the future segment as target.

However, this training protocol creates a critical mismatch with real-world deployment. In practice, forecasting systems operate in a *rolling* manner: at each time step, predictions are made for the future, and ground truth for the current step becomes available shortly after. This sequential revelation of outcomes yields a stream of *past prediction residuals*—a rich, causal signal that reflects the model’s recent performance and systematic biases.

Despite its availability and relevance, this residual signal is *not used during training* in standard deep forecasting pipelines. Models are optimized to minimize point-wise loss on isolated segments, with no mechanism to learn how to interpret or leverage their own past errors for future correction. Consequently, even when residuals clearly indicate persistent over- or under-prediction, the model remains “blind” to this feedback during inference.

As a result, we propose TEFL (Temporal Error Feedback Learning), a general framework that explicitly incorporates past prediction residuals from rolling forecasts into the forecasting process—during both training and evaluation. Formally, the forecasts for time step t are obtained as:

$$\hat{y}_t = f([y_{t-1}, \dots, y_{t-p}]) + g([\epsilon_{t-1}, \dots, \epsilon_{t-q}]), \quad (1)$$

In this formulation, y_t is the time series value at time t , p and q denote the lengths of the observation window and the error feedback window, respectively. The functions f and g are parameterized as neural networks (e.g., Transformer or MLP).

Despite its simplicity, implementing this idea in modern deep forecasting faces three challenges:

- **Error Selection:** In multi-step forecasting, the pre-

diction error at each time step is a vector of length k , but only a prefix of it is observable at next time. We define a selection rule that identifies which errors can be reliably used as feedback signals, ensuring temporal consistency and full observability.

- **Integration Design:** To avoid interfering with the base forecaster, we design a decoupled correction module that adds a small adjustment signal—computed solely from historical errors—to the base prediction. This design ensures minimal computational overhead and compatibility with different model architectures.
- **Training the base model and the error-integration module:** Joint training is unstable because the error module relies on predictions from the base model, which may be inaccurate early in training. We address this with a two-stage strategy: first warm up the base model to produce reliable errors, then jointly fine-tune both components.

As a result, we propose **TEFL** (Temporal Error Feedback Learning), a general and lightweight framework that enables deep forecasters to learn from their own historical residuals. This design provides consistent improvements across diverse forecasting scenarios:

- **Improved baseline accuracy:** On standard benchmark dataset, residual feedback corrects systematic biases, reducing MAE by 5–10%.
- **Adaptation under distribution shifts:** When the data distribution changes (e.g., seasonal transitions), recent residuals automatically adjust forecasts without retraining.
- **Robustness to abrupt shocks:** Large errors from anomalies are directly propagated to subsequent predictions, mitigating error propagation.

We summarize the contributions of our work as follows.

1. We identify and formalize the training-deployment mismatch caused by ignoring rolling-residual feedback in deep time series forecasting.
2. We propose TEFL, a general framework with principled solutions to error observability, architectural integration, and training stability.
3. We demonstrate TEFL’s effectiveness and compatibility across a wide range of models and datasets.

2. Related work

2.1. Deep learning based time series prediction model

In recent years, deep learning has become the dominant approach in time series forecasting, with various model architectures proposed to capture complex dependencies in sequential data. Transformer-based models, such as Informer (Zhou et al., 2021), PatchTST (Nie et al., 2023), and iTransformer (Liu et al., 2023), excel at modeling long-term temporal dependencies through attention mechanisms. They further improve efficiency and performance with techniques like sparse attention, series patching, and channel-independent embeddings (Zhou et al., 2021). Meanwhile, CNN-based models (e.g., TimesNet) (Wu et al., 2022; Huang et al., 2024) are effective at extracting local and periodic patterns, while MLP-based models (e.g., DLinear (Zeng et al., 2023), TimeMixer (Wang et al., 2024b)) offer lightweight and efficient solutions with multi-scale processing.

Regarding training strategies, traditional methods typically compute regression losses (e.g., MSE/MAE) uniformly over the whole sequence. Recently, researchers have started to explore more refined training paradigms. For example, curriculum learning (Wu et al., 2020) gradually increases the forecasting horizon to adjust the training difficulty, while selective learning (Fu et al., 2025) goes further by identifying and masking time points in the target sequence that are less generalizable. Other work replaces the standard loss with alternatives such as Dynamic Time Warping (Cuturi & Blondel, 2017), frequency-domain loss (Wang et al., 2024a), or distribution matching (Kudrat et al., 2025), aiming to better align predicted and target sequences in terms of temporal or spectral shapes. However, a common limitation across these approaches is that they treat each training segment in isolation, without leveraging the natural feedback loop present in real-world rolling forecasting—where past prediction residuals become available sequentially and could inform future predictions. As a result, even when systematic biases emerge during evaluation, the model has no mechanism to learn from or correct them.

2.2. Forecasting with historical prediction residuals

A line of prior work has explored using historical prediction residuals to improve forecasting accuracy. While conceptually related to our approach, they differ fundamentally in assumptions, training protocol, and applicability to modern deep forecasting.

(1) Two-stage residual modeling with shallow models

Early hybrid approaches follow a two-stage pipeline: first, a simple linear forecaster—such as an AR or ARIMA model—is fitted to the time series; then, a machine learning model (e.g., neural networks (Zhang, 2003), support vector

machines (Nie et al., 2012), or ensemble methods (Khashei & Bijari, 2011)) is trained to model the residuals from the linear model. This decoupled training is effective only when the base model is low-capacity and not prone to overfitting, ensuring that training residuals reflect true error patterns. In contrast, when the base model is a high-capacity deep network, training-set residuals become unreliable due to overfitting, leading to poor generalization of the residual model. Moreover, these methods cannot handle multi-step forecasting, where only a prefix of past errors is observable. This limitation highlights the need for joint training and causally consistent error selection.

(2) Statistical modeling under autocorrelated errors In the statistics literature, several works study model estimation under autocorrelated errors—a setting where standard estimation assumptions break down. For example, Xiao et al. (2003) proposed a pre-whitening strategy; Chen et al. (2015) studied varying-coefficient models under error autocorrelation; Lei et al. (2016) used B-splines with Whittle likelihood for joint estimation; Oliveira & Paula (2021) combined penalized splines with autoregressive structures; and Liu & Yin (2022) introduced B-spline-based generalized least squares for correlated errors. While some employ iterative or two-stage estimation strategies that loosely inspire our warm-up + fine-tuning design, they focus on parameter estimation rather than predictive performance, assume smooth functional forms, and do not support deep architectures or rolling multi-horizon forecasting.

(3) Classical error-feedback mechanisms in time series prediction The use of past prediction errors for correction is not new—it lies at the heart of several foundational frameworks in statistical time series analysis. In the Box–Jenkins paradigm, significant autocorrelation in AR model residuals motivates the inclusion of moving-average terms, yielding ARMA models whose optimal predictors explicitly incorporate lagged residuals (Bartholomew, 1971). Similarly, the Kalman filter in linear state-space models updates its state estimate by feeding back the one-step-ahead innovation (i.e., prediction error) scaled by an optimal gain derived from the system’s noise structure (Durbin & Koopman, 2012). These approaches provide principled, theoretically optimal solutions—but only under strong parametric assumptions (linearity, Gaussianity, known dynamics). Crucially, error feedback is embedded within the model specification, making it non-modular and inapplicable to black-box or deep forecasters. Our work revisits this classical insight as a universal post-hoc correction, decoupling the feedback mechanism from model internals while preserving its core benefit.

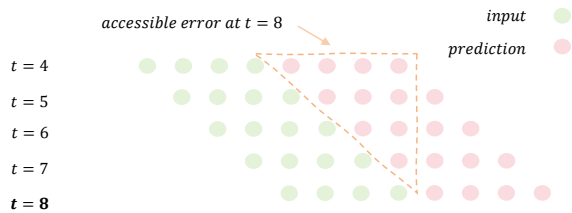


Figure 1. Example of historical errors

3. Method

3.1. Selection of historical prediction errors

In rolling multi-step forecasting, the model predicts a full horizon (e.g., 96 steps) at each time step. However, only the immediate next observation becomes available in real time. This means that, at time t , the only prediction errors available for feedback are those from forecasts made at or before time $t - H$, where H is the prediction horizon—because only then has the full ground truth become observable.

To respect this causality constraint during training, we must select historical errors that would be genuinely available in a real rolling deployment. As illustrated in Figure 1, consider a case where the model forecasts 4 steps ahead. At time $t = 8$, only the prediction errors marked by the triangular region have already been observed—and therefore, only those errors can be used for training.

Within this feasible set, our method adopts a simple yet effective strategy: we use the complete error vector from exactly one horizon ago, i.e., the errors produced at time $t - H$, whose predictions cover steps $t - H + 1$ through t . This choice aligns with the natural rhythm of rolling forecasting—after issuing a H -step forecast, the system waits H steps to receive full feedback before making the next prediction. By mirroring this delay, our training protocol better simulates the temporal structure of real-world deployment.

Moreover, using the full error vector across all horizons provides richer supervisory signals than selecting only a subset (e.g., the first-step error), as it captures horizon-specific biases and correlations. While alternative selections are possible, our ablation study in Appendix G shows that the proposed delayed-full-horizon strategy consistently yields the best performance.

3.2. The design of error module

Given the selected error signals, we now turn to their integration into the forecasting process. In our framework, these errors are processed by a lightweight adapter and then added to the forecasts produced by the base model. This adapter must balance two requirements: sufficient expressive capacity and a compact parameter size to avoid overfitting. This design principle aligns with parameter-efficient fine-tuning

methods, where a pre-trained base model is frozen and only a small adapter is updated.

Inspired by the Low-Rank Adaptation (LoRA) technique (Hu et al., 2022), we implement the adapter as two low-rank projection matrices. Let the matrix of past prediction errors be denoted as $\epsilon \in \mathbb{R}^{d \times H}$ and the base model’s forecast as $\hat{y} \in \mathbb{R}^{d \times H}$, where d is the dimension of time series and H is the prediction horizon. This error ϵ is first projected into a lower-dimensional space and then mapped back to the original output dimension. The complete error module is formulated as:

$$\hat{y}' = (\text{ReLu}(\epsilon \times W_1))W_2 + \hat{y} \quad (2)$$

where \hat{y}' is the final, adjusted prediction and W_1, W_2 are two small matrices of shape $\mathbb{R}^{H \times r}$ and $\mathbb{R}^{r \times H}$, respectively. And r is much smaller than H . The use of two small matrices, W_1 and W_2 , instead of some large weight matrices, drastically reduces the number of parameters.

Although more complex modules, such as gated networks or deeper architectures, could be considered, experiments discussed in Appendix H indicate that these alternatives generally perform worse, with models containing more parameters often exhibiting poorer efficiency.

3.3. Training process

Given that our framework introduces a learnable error correction module g on top of the base forecaster f , the choice of training strategy critically affects both performance and generalization. A naive approach would be to first train the base forecaster f to convergence and then train the error module g separately using its residuals. However, this two-stage pipeline risks a distributional mismatch: the error patterns observed during training may differ significantly from those encountered during rolling evaluation, especially if f overfits to the shuffled training segments.

Conversely, jointly training f and g from scratch introduces another challenge: in early epochs, the predictions of f are highly inaccurate, causing the inputs to g (i.e., simulated residuals) to be dominated by noise. This hinders the error module’s ability to learn meaningful correction strategies.

To balance these concerns, we adopt a two-phase training protocol that ensures both signal quality and parameter co-adaptation.

3.3.1. PHASE 1: WARM-UP WITH TEMPORALLY STRUCTURED RESIDUALS

We first warm up the base model f using a composite loss that encourages its prediction residuals to exhibit temporal structure rather than white noise. The rationale is simple: if residuals are purely random, they carry no predictable signal for the error module; but if they retain systematic

patterns (e.g., due to distribution shift or model bias), the error module can learn to correct them.

To quantify and promote such structure, we employ *spectral flatness* (SF)—a differentiable measure of how “noise-like” a time series is (Dubnov, 2004; Gray & Markel, 2003). For a residual sequence $\epsilon = [\epsilon_0, \dots, \epsilon_{b-1}]$ over b consecutive time steps, SF is computed as follows. First, apply the Discrete Fourier Transform (DFT):

$$E_k = \sum_{n=0}^{b-1} \epsilon_n e^{-2\pi i k n / b}, \quad k = 0, \dots, b-1. \quad (3)$$

Then compute the power spectrum $P_k = |E_k|^2$, and define spectral flatness as the ratio of its geometric mean to arithmetic mean:

$$\text{SF}(\epsilon) = \frac{\left(\prod_{k=0}^{b-1} P_k\right)^{1/b}}{\frac{1}{b} \sum_{k=0}^{b-1} P_k}. \quad (4)$$

When the power spectrum is uniform (as in white noise), SF approaches 1; when energy is concentrated in a few frequencies (indicating structure or periodicity), SF approaches 0. By minimizing SF during warm-up, we encourage residuals to deviate from white noise and retain temporal dependencies. Crucially, this requires training on temporally contiguous segments without shuffling, as spectral structure is only meaningful in the correct time order. Accordingly, our Phase 1 dataloader preserves the original sequence ordering.

The total warm-up loss for a batch of consecutive samples is:

$$\mathcal{L}_{\text{warm}} = \ell(y, \hat{y}) + \alpha \cdot \text{SF}(y - \hat{y}), \quad (5)$$

where ℓ is the standard forecasting loss (e.g., MAE), and $\alpha > 0$ controls the regularization strength.

3.3.2. PHASE 2: JOINT TRAINING WITH CAUSAL ERROR SIMULATION

In the second phase, we jointly optimize the base model f and the error module g . For clarity, we assume a standard forecasting setting where both the input (lookback) window and the output (prediction) horizon have the same length H —a common configuration in many time series benchmarks (e.g., predicting the next 96 steps given the past 96 steps).

Under this setting, to simulate the causal structure of rolling forecasting within a batch-compatible framework, each training sample is constructed from a contiguous segment of length $3H$, covering time steps $t - 2H$ through $t + H - 1$. This segment is partitioned into three consecutive blocks:

- **Context window** (X_{ctx}): $[y_{t-2H}, \dots, y_{t-H-1}]$ — used as input to generate a forecast for the subsequent H steps;

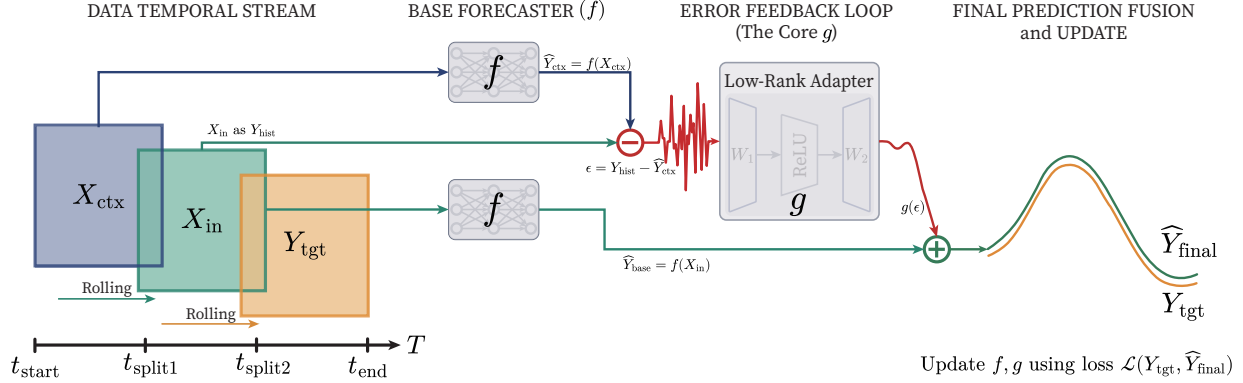


Figure 2. Illustration of TEFL joint training pipeline.

- **Input window** (X_{in}): $[y_{t-H}, \dots, y_{t-1}]$ — serves as the input for the current prediction;
- **Target** (Y_{tgt}): $[y_t, \dots, y_{t+H-1}]$ — the ground-truth values to be predicted.

The training procedure proceeds as follows:

1. Apply the base model f to X_{ctx} to obtain a prediction $\hat{y}_{t-H:t-1}$ for time steps $t-H$ through $t-1$.
2. Compute the residual vector $\epsilon = y_{t-H:t-1} - \hat{y}_{t-H:t-1}$, where $y_{t-H:t-1} = [y_{t-H}, \dots, y_{t-1}]$ are the true observations. This error corresponds to a full H -step forecast at time $t-H$, and would be fully observable by time t in a real rolling deployment.
3. Apply f to X_{in} to produce the base forecast $\hat{y}_{t:t+H-1}$ for the target horizon.
4. Pass ϵ through the error module g and add its output as a correction:

$$\hat{y}'_{t:t+H-1} = f(X_{in}) + g(\epsilon). \quad (6)$$
5. Compute the loss between $\hat{y}'_{t:t+H-1}$ and $Y_{tgt} = y_{t:t+H-1}$, and backpropagate gradients through both f and g .

This construction ensures two critical properties:

1. **Causal validity:** The error signal ϵ is derived from a forecast whose entire ground truth is available at the time of the current prediction—respecting the temporal constraints of online evaluation.
2. **Parameter consistency:** Since ϵ is computed using the current version of f , there is no mismatch between the error and the model state.

Although our current implementation assumes equal input and output lengths (H), the core idea—using a fully observed error block for feedback—can be generalized to asymmetric settings with minor adjustments. The complete workflow is illustrated in Figure 2. Ablation studies on the role of spectral flatness regularization, as well as comparisons with alternative training strategies are provided in Appendix F.

4. Theoretical Justification

While our practical implementation employs highly nonlinear neural forecasters, a rigorous theoretical analysis of such models remains intractable. Nevertheless, the core mechanism behind TEFL can be rigorously demonstrated in an idealized setting: even an *oracle* forecaster—one that computes the true conditional expectation—produces residuals with exploitable temporal structure, provided that (i) predictions are made using a finite input window (ii) the underlying system exhibits nonlinear state transitions, and (iii) observations are corrupted by additive noise. Under these conditions, observation noise obscures the true latent state, causing the optimal predictor to make systematic errors whose magnitude and sign depend on past noise realizations. As a result, the residual sequence exhibits temporal correlations—not due to model misspecification, but as an inherent consequence of partial observability in nonlinear systems. Crucially, this structure can be leveraged for correction. As we show below, even a simple linear adapter can exploit these correlations to improve forecasting accuracy.

We analyze TEFL under a canonical nonlinear Gaussian state-space model:

$$x_t = f(x_{t-1}) + \eta_{t-1}, \quad \eta_{t-1} \sim \mathcal{N}(0, \sigma_\eta^2), \quad (7)$$

$$y_t = x_t + \varepsilon_t, \quad \varepsilon_t \sim \mathcal{N}(0, \sigma_\varepsilon^2), \quad (8)$$

where $f \in C^2(\mathbb{R})$, the latent process $\{x_t\}$ is stationary with invariant distribution π , and all noise variables are mutually independent. The forecaster observes only the

noisy sequence $\{y_t\}$ and uses the MSE-optimal one-step predictor $g^*(y_{t-1}) = \mathbb{E}[y_t | y_{t-1}]$.

Despite its optimality, the residual $r_t := y_t - g^*(y_{t-1})$ exhibits temporal dependence due to observation noise. The following proposition quantifies this effect.

Proposition 4.1 (Lag-1 Autocovariance of Residuals). *Consider the state-space model with observation noise ($\sigma_\varepsilon > 0$) and nonlinear dynamics such that $\mu'_f := \mathbb{E}_{x \sim \pi}[f'(x)] \neq 0$. Then the prediction residuals of the optimal one-step forecaster satisfy*

$$\text{Cov}(r_t, r_{t-1}) \neq 0.$$

Thus, even an oracle predictor leaves structured, predictable residuals whenever observations are noisy and the dynamics are nonlinear—a common condition in real-world time series.

This non-zero autocorrelation implies that using past residuals to predict future residuals can improve the predictions of g^* . We formalize this for a linear TEFL adapter: $\hat{y}_t = g^*(y_{t-1}) + \beta r_{t-1}$, where β is estimated from T samples via ordinary least squares.

Theorem 4.2 (Finite-Sample MSE Reduction). *Let $\gamma = \text{Cov}(r_t, r_{t-1})$, $V = \text{Var}(r_t)$, and assume $|\gamma| > 0$. Denote the empirical TEFL coefficient by $\hat{\beta}_T = \frac{\sum_{t=2}^T r_t r_{t-1}}{\sum_{t=2}^T r_{t-1}^2}$. Then, under some mild conditions, there exist constant $c > 0$ such that for any $\delta \in (0, 1)$, with probability at least $1 - \delta$,*

$$\begin{aligned} & \frac{1}{T-1} \sum_{t=2}^T (y_t - g^*(y_{t-1}) - \hat{\beta}_T r_{t-1})^2 \\ & \leq \frac{1}{T-1} \sum_{t=2}^T r_t^2 - \frac{\gamma^2}{V} + c \left(\sqrt{\frac{\log(1/\delta)}{T}} + \frac{(\log(1/\delta))^2}{T} \right) \end{aligned} \quad (9)$$

Hence, for sufficiently large T , TEFL strictly improves over the base predictor with high probability.

These results establish that residual feedback is theoretically justified even under *idealized conditions*: stationary dynamics, no distribution shift, and an oracle base predictor. Moreover, this performance gain can be captured using only a *linear* adapter. In practical settings—where models are misspecified, training data suffer from distribution shifts, or the base forecaster is suboptimal—the residual signal is likely to contain *even richer* information about systematic errors. Consequently, more expressive adapters (e.g., neural networks) might yield *greater* improvements in such realistic, non-stationary regimes. Our analysis focuses on one-step history for clarity, but the presence of residual autocorrelation persists under multi-step conditioning

in nonlinear or partially observed systems—a regime that covers most real-world forecasting tasks. Full proofs and additional discussion are provided in Appendix A.

5. Experiment

5.1. Set up

To verify the effectiveness of the proposed TEFL method, we conducted experiments on ten datasets. These include commonly used time series forecasting datasets such as the ETT series, Weather, Electricity, etc. We also collected one financial dataset: the EURUSD dataset, which contains 15-minute interval data on the Euro/USD exchange rate and trading volume for 2022. Detailed dataset descriptions are provided in Appendix C.

Our method is independent of the specific form of the base forecasting model. Therefore, to demonstrate its broad applicability, we selected five deep learning-based time series models: two classical models, DLinear (Zeng et al., 2023) and iTransformer (Liu et al., 2023), three recently proposed models, SOFTS (Han et al., 2024), TimesFilter (Hu et al., 2025), and Amplifier (Fei et al., 2025). All experiments are based on the open-source library TSLib (Wang et al., 2024c).

For the forecasting task, we follow previous work. The input window length is set to 96. We evaluate the models on four different output horizons: 96, 192, 336, and 720 steps. All experiments are repeated three times.

5.2. Results

Table 1 reports the results across all datasets and models. For each dataset, the upper row shows the results of the original training method, and the lower row shows the results of TEFL method. These results represent the average performance across four forecasting horizons. The final four columns of the table present the average MSE, average MAE, and the average percentage improvement for all forecasting models.

The experimental results indicate that, in terms of average MSE and MAE, the TEFL method outperforms the corresponding baseline methods on all ten datasets. The extent of performance improvement varies across datasets. The most significant improvement is observed on the CzeLan dataset, where MSE and MAE are substantially reduced by 18.1% and 13.1%, respectively. Notable improvements are also achieved on the Solar dataset (MSE: 11.9%, MAE: 13.6%). Stable improvements ranging from 5% to 9% are observed on datasets including ETTm2, AQWan, Aqsunyi, ETTm1, and Weather.

From the model perspective, the TEFL method consistently improves the performance of all five base forecasting mod-

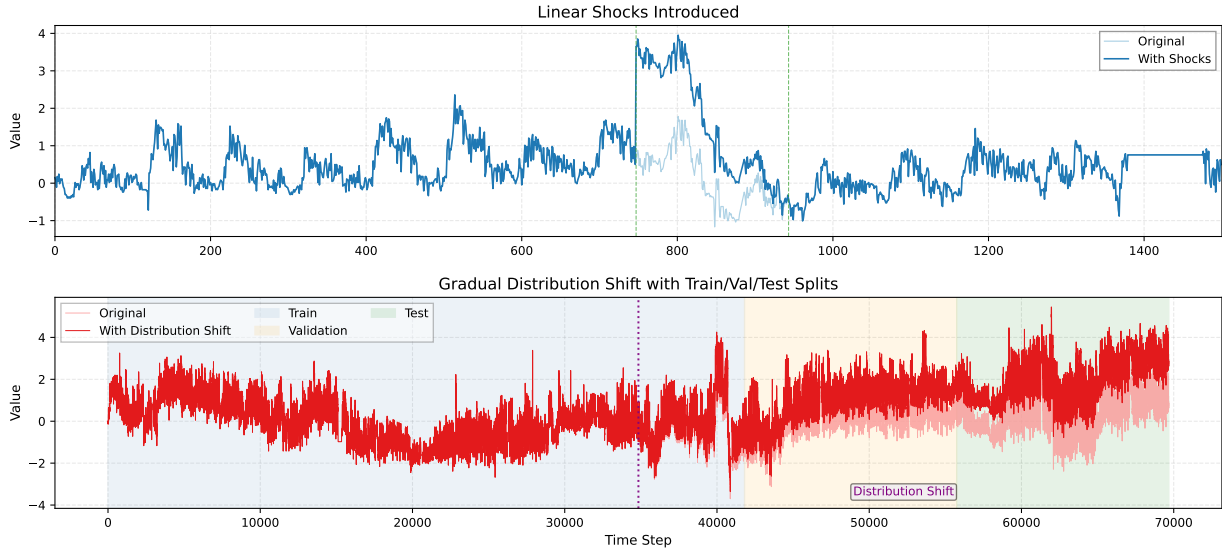


Figure 3. Examples of shock and distribution shift

Table 1. Main results. Lower is better (\downarrow). AVG denotes the average performance across five base models; IMP shows the relative improvement (%) of +TEFL over Baseline.

Model	Metric	SOFTS		iTrans		Dlinear		TimeFilter		Amplifier		AVG \downarrow		IMP	
		MSE	MAE	MSE	MAE	MSE	MAE								
ETTm1	Baseline	0.394	0.404	0.408	0.410	0.404	0.407	0.381	0.395	0.383	0.397	0.394	0.402		
	+TEFL	0.362	0.378	0.380	0.388	0.372	0.384	0.366	0.376	0.366	0.378	0.369	0.381	6.3%	5.4%
ETTm2	Baseline	0.303	0.330	0.289	0.334	0.346	0.396	0.273	0.323	0.279	0.325	0.298	0.341		
	+TEFL	0.271	0.320	0.274	0.323	0.278	0.328	0.265	0.316	0.268	0.317	0.271	0.321	9.1%	6.0%
Weather	Baseline	0.256	0.278	0.258	0.279	0.266	0.316	0.241	0.271	0.246	0.273	0.253	0.283		
	+TEFL	0.241	0.268	0.239	0.266	0.253	0.292	0.227	0.259	0.231	0.264	0.238	0.270	6.0%	4.7%
Electricity	Baseline	0.174	0.265	0.179	0.272	0.226	0.320	0.160	0.259	0.173	0.267	0.182	0.277		
	+TEFL	0.171	0.261	0.168	0.258	0.202	0.290	0.160	0.256	0.170	0.252	0.174	0.263	4.5%	4.7%
EURUSD	Baseline	0.154	0.242	0.157	0.243	0.197	0.284	0.153	0.237	0.171	0.253	0.166	0.252		
	+TEFL	0.153	0.239	0.151	0.238	0.192	0.277	0.152	0.237	0.152	0.236	0.161	0.246	3.4%	2.3%
AQWan	Baseline	0.883	0.517	0.897	0.522	0.848	0.541	0.878	0.515	0.857	0.514	0.872	0.522		
	+TEFL	0.825	0.501	0.839	0.503	0.822	0.506	0.831	0.501	0.815	0.491	0.826	0.500	5.3%	4.1%
ZafNoo	Baseline	0.584	0.472	0.577	0.470	0.520	0.472	0.592	0.478	0.719	0.573	0.599	0.493		
	+TEFL	0.551	0.454	0.556	0.457	0.513	0.450	0.564	0.466	0.544	0.448	0.545	0.455	8.9%	7.8%
AQshunyi	Baseline	0.784	0.527	0.795	0.532	0.748	0.552	0.773	0.525	0.756	0.523	0.771	0.532		
	+TEFL	0.721	0.500	0.745	0.512	0.721	0.515	0.732	0.509	0.719	0.499	0.728	0.507	5.6%	4.7%
Solar	Baseline	0.231	0.258	0.236	0.266	0.327	0.398	0.223	0.251	0.253	0.285	0.254	0.292		
	+TEFL	0.205	0.257	0.218	0.246	0.253	0.245	0.221	0.251	0.231	0.262	0.224	0.252	11.9%	13.6%
CzeLan	Baseline	0.260	0.289	0.263	0.298	0.554	0.507	0.268	0.300	0.258	0.291	0.321	0.337		
	+TEFL	0.250	0.278	0.255	0.281	0.305	0.339	0.258	0.288	0.245	0.279	0.263	0.293	18.1%	13.1%

els. This demonstrates that the optimization mechanism provided by TEFL offers good compatibility and enhancement for different types of model architectures.

5.3. Robust to Shocks

Shocks refer to sudden peaks in the time series. For example, in a series representing gold prices, an abrupt political crisis may cause a sharp immediate rise, followed by a grad-

ual stabilization or decline as the situation calms (Chen & Liu, 1993). Such sudden change could cause a significant increase in the prediction errors of recent time steps. Therefore, models that incorporate past prediction errors can directly use the change as input for forecasting future values, thereby improving prediction accuracy during shock periods.

To verify this, we conducted additional experiments on the

Table 2. Results for shock data. Lower is better.

Dataset	Metric	ETTM1		ETTM2		Weather	
		MSE	MAE	MSE	MAE	MSE	MAE
Amplifier	Baseline	0.650	0.516	0.563	0.451	0.621	0.449
	+TEFL	0.579	0.474	0.505	0.425	0.539	0.404
iTrans	Baseline	0.704	0.539	0.511	0.435	0.549	0.411
	+TEFL	0.634	0.498	0.480	0.413	0.522	0.388
DLinear	Baseline	0.711	0.560	0.733	0.598	0.619	0.527
	+TEFL	0.628	0.500	0.511	0.450	0.549	0.429
SOFTS	Baseline	0.676	0.526	0.507	0.429	0.544	0.409
	+TEFL	0.618	0.493	0.471	0.402	0.501	0.372
TimeFilter	Baseline	0.625	0.503	0.508	0.429	0.522	0.400
	+TEFL	0.577	0.464	0.477	0.407	0.495	0.371
AVG	Baseline	0.673	0.529	0.564	0.468	0.571	0.440
	+TEFL	0.607	0.486	0.489	0.419	0.521	0.393
IMP (%)		9.8%	8.1%	13.4%	10.5%	8.7%	10.6%

Table 3. Results for data with distribution shift. Lower is better.

Dataset	Metric	ETTM1		ETTM2		Weather	
		MSE	MAE	MSE	MAE	MSE	MAE
Amplifier	Baseline	0.472	0.459	0.342	0.392	0.441	0.451
	+TEFL	0.435	0.429	0.283	0.340	0.286	0.333
iTrans	Baseline	0.531	0.508	0.310	0.384	0.450	0.443
	+TEFL	0.492	0.485	0.273	0.344	0.367	0.395
DLinear	Baseline	0.589	0.565	0.358	0.428	0.562	0.571
	+TEFL	0.433	0.438	0.277	0.337	0.308	0.351
SOFTS	Baseline	0.584	0.539	0.417	0.434	0.449	0.446
	+TEFL	0.483	0.473	0.291	0.364	0.408	0.423
TimeFilter	Baseline	0.662	0.603	0.373	0.412	0.389	0.427
	+TEFL	0.534	0.503	0.277	0.344	0.332	0.382
AVG	Baseline	0.568	0.535	0.360	0.410	0.458	0.468
	+TEFL	0.476	0.466	0.280	0.346	0.340	0.377
IMP (%)		16.2%	13.0%	22.2%	15.7%	25.7%	19.5%

ETTM1, ETTM2 and Weather datasets. Specifically, we artificially added 30 shocks into each dataset. Each shock lasts for 192 time steps and decays linearly, as illustrated in the upper subfigure of Figure 3. We retrained and tested both the baseline method and the TEFL method on these modified datasets. The results are presented in Table 2. For every model on these shock datasets, TEFL yields significantly lower MSE and MAE. The "IMP" row at the bottom of Table 2 highlights an average error reduction of 9.8% for ETTM1, 13.4% for ETTM2, and 8.7% for the Weather dataset. Besides, compared to the results in Table 1, our method yields a more pronounced accuracy improvement on the dataset containing shocks, which demonstrates that incorporating past prediction errors into the current input can better handle shocks.

5.4. Robust to distribution shift

Typically, past prediction errors can partially reflect distribution shifts. Therefore, our proposed TEFL method, which incorporates previous errors into the input, should be capable of modeling distribution shifts to some extent. To verify

the robustness of our method against distribution shifts, we conducted additional experiments on the ETTM1, ETTM2, and Weather datasets.

Specifically, we artificially introduced a distribution shift into these datasets. For the normalized dataset, we applied a linearly increasing distribution shift to the latter half of the data, as shown in the lower part of Figure 3. It can be observed that a progressively more pronounced distribution shift exists from the end of the training set through to the end of the test set. We repeated experiments on these datasets. And the results are presented in Table 3.

As shown in Table 3, our method achieves a substantial improvement over directly training these models. The reduction in MAE reaches 13.0%, 15.7%, and 19.5% on the three datasets, respectively. Notably, this improvement is also larger than that observed in Table 1. This result underscores the strong adaptability of TEFL method to distribution shifts.

6. Conclusion

This paper presents TEFL, a novel training paradigm for time series forecasting that explicitly incorporates historically observed prediction errors as corrective signals during learning. By simulating the causal structure of rolling forecasting, TEFL bridges the gap between conventional shuffled-batch training and real-world deployment dynamics. Extensive experiments across diverse datasets and backbone models demonstrate that TEFL consistently improves forecasting accuracy, achieving up to 10% error reduction in several settings. Moreover, TEFL exhibits enhanced robustness to distribution shifts and abrupt changes.

Our framework offers a practical and generalizable approach to adaptive forecasting, aligning offline training with online evaluation. Future directions include extending the error feedback mechanism to online learning, developing more effective training strategies, and applying this paradigm to other sequential prediction tasks such as spatiotemporal modeling.

Impact Statement

This paper presents work whose goal is to advance the field of Machine Learning. There are many potential societal consequences of our work, none which we feel must be specifically highlighted here.

References

Bai, G., Ling, C., and Zhao, L. Temporal domain generalization with drift-aware dynamic neural networks. *arXiv preprint arXiv:2205.10664*, 2022.

- Bartholomew, D. J. *Time Series Analysis Forecasting and Control*. JSTOR, 1971.
- Bradley, R. C. Basic properties of strong mixing conditions. a survey and some open questions. *arXiv Mathematics e-prints*, 2005.
- Cai, Z., Bai, G., Jiang, R., Song, X., and Zhao, L. Continuous temporal domain generalization. *Advances in Neural Information Processing Systems*, 37:127987–128014, 2024.
- Chen, C. and Liu, L.-M. Joint estimation of model parameters and outlier effects in time series. *Journal of the American Statistical Association*, 88(421):284–297, 1993.
- Chen, Z., Li, R., and Li, Y. Varying coefficient models for data with auto-correlated error process. *Statistica Sinica*, 25(2):709, 2015.
- Cuturi, M. and Blondel, M. Soft-dtw: a differentiable loss function for time-series. In *International conference on machine learning*, pp. 894–903. PMLR, 2017.
- Dubnov, S. Generalization of spectral flatness measure for non-gaussian linear processes. *IEEE Signal Processing Letters*, 11(8):698–701, 2004.
- Durbin, J. and Koopman, S. J. *Time series analysis by state space methods*. Oxford university press, 2012.
- Fei, J., Yi, K., Fan, W., Zhang, Q., and Niu, Z. Amplifier: Bringing attention to neglected low-energy components in time series forecasting. In *Proceedings of the AAAI Conference on Artificial Intelligence*, volume 39, pp. 11645–11653, 2025.
- Fu, Y., Shao, Z., Yu, C., Li, Y., An, Z., Wang, Q., Xu, Y., and Wang, F. Selective learning for deep time series forecasting. *arXiv preprint arXiv:2510.25207*, 2025.
- Gray, A. and Markel, J. A spectral-flatness measure for studying the autocorrelation method of linear prediction of speech analysis. *IEEE Transactions on Acoustics, Speech, and Signal Processing*, 22(3):207–217, 2003.
- Gruca, A., Serva, F., Lliso, L., Rípodas, P., Calbet, X., Herruzo, P., Pihrt, J., Raevskiy, R., Šimánek, P., Choma, M., et al. Weather4cast at neurips 2022: Super-resolution rain movie prediction under spatio-temporal shifts. In *NeurIPS 2022 Competition Track*, pp. 292–313. PMLR, 2023.
- Guo, P., Jin, P., Li, Z., Bai, L., and Zhang, Y. Online test-time adaptation of spatial-temporal traffic flow forecasting. *arXiv preprint arXiv:2401.04148*, 2024.
- Han, L., Chen, X.-Y., Ye, H.-J., and Zhan, D.-C. Softs: Efficient multivariate time series forecasting with series-core fusion. *Advances in Neural Information Processing Systems*, 37:64145–64175, 2024.
- Hu, E. J., Shen, Y., Wallis, P., Allen-Zhu, Z., Li, Y., Wang, S., Wang, L., Chen, W., et al. Lora: Low-rank adaptation of large language models. *ICLR*, 1(2):3, 2022.
- Hu, Y., Zhang, G., Liu, P., Lan, D., Li, N., Cheng, D., Dai, T., Xia, S.-T., and Pan, S. Timefilter: Patch-specific spatial-temporal graph filtration for time series forecasting. *arXiv preprint arXiv:2501.13041*, 2025.
- Huang, X., Yang, C., and Yuan, Q. Leveraging intra-period and inter-period features for enhanced passenger flow prediction of subway stations. *arXiv preprint arXiv:2410.14727*, 2024.
- Huang, X., Qiu, S., Du, J., and Yang, C. Online time series prediction using feature adjustment. *arXiv preprint arXiv:2509.03810*, 2025.
- Kadiyala, A. and Kumar, A. Vector time series models for prediction of air quality inside a public transportation bus using available software. *Environmental Progress & Sustainable Energy*, 33(4):1069–1073, 2014.
- Khashei, M. and Bijari, M. A novel hybridization of artificial neural networks and arima models for time series forecasting. *Applied soft computing*, 11(2):2664–2675, 2011.
- Kudrat, D., Xie, Z., Sun, Y., Jia, T., and Hu, Q. Patch-wise structural loss for time series forecasting. *arXiv preprint arXiv:2503.00877*, 2025.
- Lau, Y.-y. A., Shao, Z., and Yeung, D.-Y. Fast and slow streams for online time series forecasting without information leakage. In *The Thirteenth International Conference on Learning Representations*, 2025.
- Lee, T. L., Toner, W., Singh, R., Joosen, A., and Asenov, M. Lightweight online adaption for time series foundation model forecasts. *arXiv preprint arXiv:2502.12920*, 2025.
- Lei, H., Xia, Y., and Qin, X. Estimation of semivarying coefficient time series models with ARMA errors. *The Annals of Statistics*, 44(4):1618 – 1660, 2016. doi: 10.1214/15-AOS1430. URL <https://doi.org/10.1214/15-AOS1430>.
- Liu, Y. and Yin, J. B-spline estimation in varying coefficient models with correlated errors. *AIMS Mathematics*, 7(3): 3509–3523, 2022.
- Liu, Y., Hu, T., Zhang, H., Wu, H., Wang, S., Ma, L., and Long, M. itransformer: Inverted transformers are

- effective for time series forecasting. *arXiv preprint arXiv:2310.06625*, 2023.
- Merlevède, F., Peligrad, M., and Rio, E. A bernstein type inequality and moderate deviations for weakly dependent sequences. *Probability Theory and Related Fields*, 151(3):435–474, 2011.
- Morid, M. A., Sheng, O. R. L., and Dunbar, J. Time series prediction using deep learning methods in healthcare. *ACM Transactions on Management Information Systems*, 14(1):1–29, 2023.
- Nasery, A., Thakur, S., Piratla, V., De, A., and Sarawagi, S. Training for the future: A simple gradient interpolation loss to generalize along time. *Advances in Neural Information Processing Systems*, 34:19198–19209, 2021.
- Nie, H., Liu, G., Liu, X., and Wang, Y. Hybrid of arima and svms for short-term load forecasting. *Energy Procedia*, 16:1455–1460, 2012.
- Nie, Y., Nguyen, N. H., Sinthong, P., and Kalagnanam, J. A time series is worth 64 words: Long-term forecasting with transformers. In *The Eleventh International Conference on Learning Representations*, 2023.
- Oliveira, R. A. and Paula, G. A. Additive models with autoregressive symmetric errors based on penalized regression splines. *Computational Statistics*, 36(4):2435–2466, 2021.
- Pham, Q., Liu, C., Sahoo, D., and Hoi, S. C. Learning fast and slow for online time series forecasting. In *ICLR*, 2023.
- Poyatos, R., Granda, V., Flo, V., Adams, M. A., Adorján, B., Aguadé, D., Aidar, M. P., Allen, S., Alvarado-Barrientos, M. S., Anderson-Teixeira, K. J., et al. Global transpiration data from sap flow measurements: the sapfluxnet database. *Earth System Science Data Discussions*, 2020: 1–57, 2020.
- Qin, T., Wang, S., and Li, H. Generalizing to evolving domains with latent structure-aware sequential autoencoder. In *International Conference on Machine Learning*, pp. 18062–18082. PMLR, 2022.
- Qiu, X., Hu, J., Zhou, L., Wu, X., Du, J., Zhang, B., Guo, C., Zhou, A., Jensen, C. S., Sheng, Z., et al. Tfb: Towards comprehensive and fair benchmarking of time series forecasting methods. *arXiv preprint arXiv:2403.20150*, 2024.
- Schirmer, M., Zhang, D., and Nalisnick, E. Temporal test-time adaptation with state-space models. *arXiv preprint arXiv:2407.12492*, 2024.
- Wang, H., Pan, L., Chen, Z., Yang, D., Zhang, S., Yang, Y., Liu, X., Li, H., and Tao, D. Fredf: Learning to forecast in the frequency domain. *arXiv preprint arXiv:2402.02399*, 2024a.
- Wang, S., Wu, H., Shi, X., Hu, T., Luo, H., Ma, L., Zhang, J. Y., and Zhou, J. Timemixer: Decomposable multi-scale mixing for time series forecasting. *arXiv preprint arXiv:2405.14616*, 2024b.
- Wang, Y., Wu, H., Dong, J., Liu, Y., Wang, C., Long, M., and Wang, J. Deep time series models: A comprehensive survey and benchmark. *arXiv preprint arXiv:2407.13278*, 2024c.
- Wen, Q., Chen, W., Sun, L., Zhang, Z., Wang, L., Jin, R., Tan, T., et al. Onenet: Enhancing time series forecasting models under concept drift by online ensembling. *Advances in Neural Information Processing Systems*, 36: 69949–69980, 2023.
- Wu, H., Hu, T., Liu, Y., Zhou, H., Wang, J., and Long, M. Timesnet: Temporal 2d-variation modeling for general time series analysis. *arXiv preprint arXiv:2210.02186*, 2022.
- Wu, Z., Pan, S., Long, G., Jiang, J., Chang, X., and Zhang, C. Connecting the dots: Multivariate time series forecasting with graph neural networks. In *Proceedings of the 26th ACM SIGKDD international conference on knowledge discovery & data mining*, pp. 753–763, 2020.
- Xiao, Z., Linton, O. B., Carroll, R. J., and Mammen, E. More efficient local polynomial estimation in nonparametric regression with autocorrelated errors. *Journal of the American Statistical Association*, 98(464):980–992, 2003.
- Yu, E., Lu, J., Yang, X., Zhang, G., and Fang, Z. Learning robust spectral dynamics for temporal domain generalization. *arXiv preprint arXiv:2505.12585*, 2025.
- Zeng, A., Chen, M., Zhang, L., and Xu, Q. Are transformers effective for time series forecasting? In *Proceedings of the AAAI conference on artificial intelligence*, volume 37, pp. 11121–11128, 2023.
- Zhang, G. P. Time series forecasting using a hybrid arima and neural network model. *Neurocomputing*, 50:159–175, 2003.
- Zhang, S., Guo, B., Dong, A., He, J., Xu, Z., and Chen, S. X. Cautionary tales on air-quality improvement in beijing. *Proceedings of the Royal Society A: Mathematical, Physical and Engineering Sciences*, 473(2205):20170457, 2017.

Zhou, H., Zhang, S., Peng, J., Zhang, S., Li, J., Xiong, H., and Zhang, W. Informer: Beyond efficient transformer for long sequence time-series forecasting. In *Proceedings of the AAAI conference on artificial intelligence*, volume 35, pp. 11106–11115, 2021.

A. Theoretical analysis

Our theoretical analysis is grounded in a canonical hidden-state time series model under observational noise. Under that setting, even for an oracle predictor— one that knows the true data-generating mechanism- the resulting prediction error on the observed sequence exhibits temporal correlation across consecutive time steps. This correlation arises from two sources: (i) the intrinsic dependence in the latent dynamics, and (ii) the persistent influence of past observation noise through the filtering history.

This implies that even an optimal predictor leaves structured, predictable residuals in the presence of observation noise. Consequently, a secondary correction mechanism that leverages recent residual history can consistently reduce prediction error, without requiring any modification to the base forecaster. This insight forms the core theoretical justification for our approach: residual-guided refinement is provably beneficial even under oracle conditions, provided the observation model is noisy and the transition dynamic is nonlinear—a ubiquitous scenario in real-world time series. In the following, we formalize this intuition in a nonlinear-Gaussian setting and establish finite-sample guarantees for residual-based correction.

Proposition A.1 (Lag-1 Autocovariance of Residuals). *Consider the scalar state-space model*

$$x_t = f(x_{t-1}) + \eta_{t-1}, \quad \eta_{t-1} \sim \mathcal{N}(0, \sigma_\eta^2), \quad (10)$$

$$y_t = x_t + \varepsilon_t, \quad \varepsilon_t \sim \mathcal{N}(0, \sigma_\varepsilon^2), \quad (11)$$

where $f \in C^2(\mathbb{R})$ has bounded first and second derivatives, $\{x_t\}$ is a geometrically ergodic Markov chain with invariant density $\pi(x) > 0$ for all $x \in \mathbb{R}$, and all noise variables are mutually independent. Define the optimal one-step predictor

$$g^*(y_{t-1}) := \mathbb{E}[y_t \mid y_{t-1}],$$

and the prediction residual

$$r_t := y_t - g^*(y_{t-1}).$$

Assume that $\mu'_f := \mathbb{E}_{x \sim \pi}[f'(x)] \neq 0$ and $\sigma_\varepsilon > 0$. Then, as $\sigma_\varepsilon \rightarrow 0$,

$$\text{Cov}(r_t, r_{t-1}) = -\mu'_f \sigma_\varepsilon^2 + o(\sigma_\varepsilon^2).$$

In particular, $\text{Cov}(r_t, r_{t-1}) \neq 0$ for all sufficiently small $\sigma_\varepsilon > 0$.

Proof. We proceed in three steps: (i) asymptotic expansion of the conditional expectation under small observation noise, (ii) decomposition of the residuals, and (iii) precise covariance calculation.

Step 1: Small-noise expansion of $\mathbb{E}[f(x) \mid y]$.

Consider the static observation model

$$x \sim \pi(x), \quad y = x + \varepsilon, \quad \varepsilon \sim \mathcal{N}(0, \sigma_\varepsilon^2),$$

with $\pi \in C^2(\mathbb{R})$, $\pi(x) > 0$, and $f \in C^2(\mathbb{R})$ having bounded derivatives up to order 2. The posterior density is

$$p(x \mid y) = \frac{\pi(x)\phi((y-x)/\sigma_\varepsilon)}{\int_{\mathbb{R}} \pi(u)\phi((y-u)/\sigma_\varepsilon) du}, \quad \text{where } \phi(z) = (2\pi)^{-1/2}e^{-z^2/2}.$$

Using the change of variable $x = y - \sigma_\varepsilon z$, we obtain

$$\mathbb{E}[f(x) \mid y] = \frac{\int_{\mathbb{R}} f(y - \sigma_\varepsilon z)\pi(y - \sigma_\varepsilon z)\phi(z) dz}{\int_{\mathbb{R}} \pi(y - \sigma_\varepsilon z)\phi(z) dz}.$$

By Taylor's theorem with remainder, for some constants $C_f, C_\pi > 0$,

$$\begin{aligned} f(y - \sigma_\varepsilon z) &= f(y) - \sigma_\varepsilon f'(y)z + \frac{1}{2}\sigma_\varepsilon^2 f''(y)z^2 + R_f(z), \\ \pi(y - \sigma_\varepsilon z) &= \pi(y) - \sigma_\varepsilon \pi'(y)z + \frac{1}{2}\sigma_\varepsilon^2 \pi''(y)z^2 + R_\pi(z), \end{aligned}$$

where $|R_f(z)| \leq C_f \sigma_\varepsilon^3 |z|^3$ and $|R_\pi(z)| \leq C_\pi \sigma_\varepsilon^3 |z|^3$.

Since $\mathbb{E}_\phi[z] = 0$, $\mathbb{E}_\phi[z^2] = 1$, and $\mathbb{E}_\phi[|z|^3] < \infty$, integration against $\phi(z)$ yields

$$\begin{aligned} \text{Denominator} &= \pi(y) + \frac{1}{2}\sigma_\varepsilon^2 \pi''(y) + O(\sigma_\varepsilon^3), \\ \text{Numerator} &= f(y)\pi(y) + \sigma_\varepsilon^2 \left(\frac{1}{2}f''(y)\pi(y) + f'(y)\pi'(y) \right) + O(\sigma_\varepsilon^3). \end{aligned}$$

Dividing and using $(a + \delta)/(b + \epsilon) = a/b + (\delta b - a\epsilon)/b^2 + O(\delta^2 + \epsilon^2)$, we obtain the pointwise expansion

$$\mathbb{E}[f(x) | y] = f(y) + \sigma_\varepsilon^2 \left(\frac{1}{2}f''(y) + f'(y) \frac{\pi'(y)}{\pi(y)} \right) + O(\sigma_\varepsilon^3), \quad (12)$$

valid for all $y \in \mathbb{R}$, with the remainder uniform on compact sets. Since π is the stationary density of a geometrically ergodic chain and f' is bounded, all expectations below are well-defined.

Step 2: Residual decomposition.

Recall that $y_t = f(x_{t-1}) + \eta_{t-1} + \varepsilon_t$, so

$$r_t = y_t - \mathbb{E}[y_t | y_{t-1}] = f(x_{t-1}) - \mathbb{E}[f(x_{t-1}) | y_{t-1}] + \eta_{t-1} + \varepsilon_t.$$

Since $y_{t-1} = x_{t-1} + \varepsilon_{t-1}$, we may write $x_{t-1} = y_{t-1} - \varepsilon_{t-1}$. Applying Taylor's theorem to f around y_{t-1} gives

$$f(x_{t-1}) = f(y_{t-1}) - f'(y_{t-1})\varepsilon_{t-1} + \frac{1}{2}f''(y_{t-1})\varepsilon_{t-1}^2 + O_p(\sigma_\varepsilon^3).$$

On the other hand, by the small-noise expansion (12),

$$\mathbb{E}[f(x_{t-1}) | y_{t-1}] = f(y_{t-1}) + O(\sigma_\varepsilon^2).$$

Subtracting these two expressions yields

$$f(x_{t-1}) - \mathbb{E}[f(x_{t-1}) | y_{t-1}] = -f'(y_{t-1})\varepsilon_{t-1} + O_p(\sigma_\varepsilon^2).$$

Therefore, the residual admits the asymptotic representation

$$r_t = -f'(y_{t-1})\varepsilon_{t-1} + \eta_{t-1} + \varepsilon_t + O_p(\sigma_\varepsilon^2). \quad (13)$$

Analogously,

$$r_{t-1} = -f'(y_{t-2})\varepsilon_{t-2} + \eta_{t-2} + \varepsilon_{t-1} + O_p(\sigma_\varepsilon^2). \quad (14)$$

Step 3: Covariance calculation.

Since $\mathbb{E}[r_t] = \mathbb{E}[r_{t-1}] = 0$ by construction of the optimal predictor, we have

$$\text{Cov}(r_t, r_{t-1}) = \mathbb{E}[r_t r_{t-1}].$$

Substituting the expansions (13) and (14), and using the mutual independence of all noise variables across time (in particular, ε_s, η_s are independent of $\{y_u : u \leq s-1\}$), we observe that all cross terms vanish in expectation except those involving the same noise instance.

The only non-vanishing contribution at order σ_ε^2 arises from the product of $-f'(y_{t-1})\varepsilon_{t-1}$ (from r_t) and ε_{t-1} (from r_{t-1}). All other products involve independent zero-mean random variables or higher-order remainders. Hence,

$$\mathbb{E}[r_t r_{t-1}] = \mathbb{E}[-f'(y_{t-1})\varepsilon_{t-1} \cdot \varepsilon_{t-1}] + o(\sigma_\varepsilon^2) = -\mathbb{E}[f'(y_{t-1})\varepsilon_{t-1}^2] + o(\sigma_\varepsilon^2).$$

Since $y_{t-1} = x_{t-1} + \varepsilon_{t-1}$, expanding f' around x_{t-1} ,

$$f'(x_{t-1} + \varepsilon_{t-1}) = f'(x_{t-1}) + f''(x_{t-1})\varepsilon_{t-1} + O_p(\sigma_\varepsilon^2),$$

and using $\mathbb{E}[\varepsilon_{t-1}] = 0$, $\mathbb{E}[\varepsilon_{t-1}^2] = \sigma_\varepsilon^2$, $\mathbb{E}[\varepsilon_{t-1}^3] = 0$, we obtain

$$\mathbb{E}[f'(x_{t-1} + \varepsilon_{t-1})\varepsilon_{t-1}^2] = f'(x_{t-1})\sigma_\varepsilon^2 + O(\sigma_\varepsilon^4).$$

Taking expectation over the stationary distribution π of x_{t-1} yields

$$\mathbb{E}[f'(y_{t-1})\varepsilon_{t-1}^2] = \mathbb{E}_{x \sim \pi}[f'(x)]\sigma_\varepsilon^2 + o(\sigma_\varepsilon^2).$$

Combining the above, we conclude

$$\text{Cov}(r_t, r_{t-1}) = -\mu'_f \sigma_\varepsilon^2 + o(\sigma_\varepsilon^2), \quad \text{where } \mu'_f := \mathbb{E}_{x \sim \pi}[f'(x)].$$

In particular, if f is nonlinear and the stationary measure π is non-degenerate, then $\mu'_f \neq 0$ in general, implying $\text{Cov}(r_t, r_{t-1}) \neq 0$ for all sufficiently small $\sigma_\varepsilon > 0$. \square

A.1. Finite-Sample Guarantee for Linear TEFL

Theorem A.2 (Finite-Sample MSE Reduction by TEFL). *Consider the nonlinear Gaussian state-space model:*

$$x_t = f(x_{t-1}) + \eta_{t-1}, \quad y_t = x_t + \varepsilon_t,$$

where $f \in C^2(\mathbb{R})$, $\eta_t \sim \mathcal{N}(0, \sigma_\eta^2)$, and $\varepsilon_t \sim \mathcal{N}(0, \sigma_\varepsilon^2)$ are mutually independent. Assume $|f'(x)| \leq L < 1$ for all $x \in \mathbb{R}$, then, the joint process $\{(x_t, y_t)\}_{t \geq 0}$ is stationary and geometrically ergodic. Additionally, we assume r_t is subgaussian and the stationary distribution of x_t , denoted as $\pi(x)$ is also subgaussian. Define the base predictor $\hat{y}_t^{\text{base}} = g^*(y_{t-1})$ and its residual $r_t = y_t - g^*(y_{t-1})$. The TEFL predictor employs a linear adapter:

$$\hat{y}_t^{\text{TEFL}} = g^*(y_{t-1}) + \beta r_{t-1},$$

with the empirical coefficient computed from T observations as

$$\hat{\beta}_T = \frac{\sum_{t=2}^T r_t r_{t-1}}{\sum_{t=2}^T r_{t-1}^2}.$$

Let the population quantities be

$$\gamma := \text{Cov}(r_t, r_{t-1}), V := \text{Var}(r_t), \rho_1 := \frac{\gamma}{V}.$$

Assume $V > 0$ and $|\rho_1| > 0$ —conditions satisfied whenever f is nonlinear and $\sigma_\varepsilon > 0$.

Then there exist constants $c > 0$, depending only on the geometric ergodicity rate of $\{r_t\}$ and the noise variances, such that for any $\delta \in (0, 1)$, with probability at least $1 - \delta$,

$$\frac{1}{T-1} \sum_{t=2}^T (y_t - g^*(y_{t-1}) - \hat{\beta}_T r_{t-1})^2 \leq \underbrace{\frac{1}{T-1} \sum_{t=2}^T r_t^2 - V \rho_1^2}_{\text{Base MSE}} + c \left(\sqrt{\frac{\log(1/\delta)}{T}} + \frac{(\log(1/\delta))^2}{T} \right) \quad (15)$$

In particular, for sufficiently large T , the right-hand side is strictly smaller than the base MSE with high probability.

Proof. Step 1: Error decomposition.

Let $\beta^* = \gamma/V$. A standard algebraic identity yields

$$\frac{1}{T-1} \sum_{t=2}^T (r_t - \hat{\beta}_T r_{t-1})^2 = (\mathbf{A}) + (\hat{\beta}_T - \beta^*)^2 (\mathbf{B}) + 2(\hat{\beta}_T - \beta^*) (\mathbf{C}),$$

where

$$(\mathbf{A}) = \frac{1}{T-1} \sum_{t=2}^T (r_t - \beta^* r_{t-1})^2, \quad (\mathbf{B}) = \frac{1}{T-1} \sum_{t=2}^T r_{t-1}^2, \quad (\mathbf{C}) = \frac{1}{T-1} \sum_{t=2}^T (r_t - \beta^* r_{t-1}) r_{t-1}.$$

By construction of β^* , we have $\mathbb{E}[(\mathbf{C})] = 0$ and $\mathbb{E}[(\mathbf{A})] = V - \gamma^2/V = V(1 - \rho_1^2)$.

Step 2: Mixing.

We define $X_t = (x_t, \epsilon_t)$, then X_t is stationary and geometrically ergodic, as a result, (X_t, X_{t-1}) is also stationary and geometrically ergodic. According to Theorem 3.1 in [Bradley \(2005\)](#), (X_t, X_{t-1}) is β -mixing. r_t is a measurable function of (X_t, X_{t-1}) , as a result, is also β -mixing.

Besides, the residual process $r_t = y_t - g^*(y_{t-1}) = x_t + \epsilon_t - g^*(y_{t-1})$ is subgaussian. Therefore:

$$U_t = r_t r_{t-1} - \gamma, \quad V_t = r_{t-1}^2 - V, \quad W_t = (r_t - \beta^* r_{t-1}) r_{t-1}$$

are stationary, exponentially β -mixing, and sub-exponential.

Step 3: Concentration inequalities.

By Theorem 1 of [Merlevède et al. \(2011\)](#), for any $\delta \in (0, 1)$, there exists a constant $c > 0$, depending only on the mixing rate and sub-exponential norms, such that with probability at least $1 - \delta$,

$$\max \left\{ \left| \frac{1}{T-1} \sum_{t=2}^T U_t \right|, \left| \frac{1}{T-1} \sum_{t=2}^T V_t \right|, \left| \frac{1}{T-1} \sum_{t=2}^T W_t \right| \right\} \leq c \left(\sqrt{\frac{\log(1/\delta)}{T}} + \frac{(\log(1/\delta))^2}{T} \right).$$

Denote this upper bound by

$$\Delta_T := c \left(\sqrt{\frac{\log(1/\delta)}{T}} + \frac{(\log(1/\delta))^2}{T} \right).$$

On this event, we have

$$\left| \frac{1}{T-1} \sum_{t=2}^T r_t r_{t-1} - \gamma \right| \leq \Delta_T, \quad \left| \frac{1}{T-1} \sum_{t=2}^T r_{t-1}^2 - V \right| \leq \Delta_T.$$

Since $V > 0$, for T large enough such that $\Delta_T < V/2$, it follows that

$$|\hat{\beta}_T - \beta^*| = \left| \frac{\frac{1}{T-1} \sum r_t r_{t-1}}{\frac{1}{T-1} \sum r_{t-1}^2} - \frac{\gamma}{V} \right| \leq \frac{V\Delta_T + |\gamma|\Delta_T}{V(V - \Delta_T)} \leq \frac{2(V + |\gamma|)}{V^2} \Delta_T =: C_0 \Delta_T.$$

Moreover,

$$|(A) - \mathbb{E}[(A)]| \leq \Delta_T, \quad |(B) - V| \leq \Delta_T, \quad |(C)| \leq \Delta_T.$$

Step 4: Final bound.

Substituting into the error decomposition gives, with probability at least $1 - \delta$,

$$\begin{aligned} \frac{1}{T-1} \sum_{t=2}^T (r_t - \hat{\beta}_T r_{t-1})^2 &\leq \mathbb{E}[(A)] + \Delta_T + (C_0 \Delta_T)^2 (V + \Delta_T) + 2C_0 \Delta_T \cdot \Delta_T \\ &\leq V(1 - \rho_1^2) + \Delta_T + C_1 \Delta_T^2, \end{aligned}$$

Note that

$$\frac{1}{T-1} \sum_{t=2}^T r_t^2 = V + \xi_T,$$

with $|\xi_T| \leq \Delta_T$ on the same high-probability event.

Then,

$$\frac{1}{T-1} \sum_{t=2}^T (r_t - \hat{\beta}_T r_{t-1})^2 \leq \frac{1}{T-1} \sum_{t=2}^T r_t^2 - V\rho_1^2 + \Delta_T + C_1 \Delta_T^2$$

The quadratic term Δ_T^2 is dominated by Δ_T for all sufficiently large T , and can thus be absorbed into the leading-order error term. Hence, there exists an constant c such that the finite-sample excess risk bound takes the simplified form shown in (15). □

This result shows that TEFL achieves a non-vanishing MSE reduction of $\gamma^2/V = \rho_1^2 V$ in expectation, and this gain dominates the $\mathcal{O}(1/\sqrt{T})$ estimation error with high probability for sufficiently large T . Moreover, the magnitude of this in-sample improvement closely matches that of the generalization error $\mathbb{E}[(y_{T+1} - \hat{y}_{T+1}^{\text{TEFL}})^2]$, differing only by higher-order terms that vanish as $T \rightarrow \infty$.

A.2. Theorem 1 in Merlevède et al. (2011)

We first recall the truncation function used in the statement of the theorem.

For any $M > 0$, define the truncation function $\phi_M : \mathbb{R} \rightarrow \mathbb{R}$ by

$$\phi_M(x) = (x \wedge M) \vee (-M).$$

Let $(X_j)_{j \in \mathbb{Z}}$ be a sequence of centered real-valued random variables. Define the quantity

$$V := \sup_{M>0} \sup_{i>0} \left(\text{Var}(\phi_M(X_i)) + 2 \sum_{j>i} |\text{Cov}(\phi_M(X_i), \phi_M(X_j))| \right). \quad (16)$$

Assume the following conditions hold:

1. There exist constants $a > 0$, $c > 0$, and $\gamma_1 > 0$ such that the τ -mixing coefficients satisfy

$$\tau(x) \leq a \exp(-cx^{\gamma_1}) \quad \text{for all } x \geq 1,$$

2. There exist constants $b > 0$ and $\gamma_2 \in (0, \infty]$ such that

$$\sup_{k>0} \mathbb{P}(|X_k| > t) \leq \exp(1 - (t/b)^{\gamma_2}) \quad \text{for all } t > 0.$$

3. Define $\gamma > 0$ by

$$\frac{1}{\gamma} = \frac{1}{\gamma_1} + \frac{1}{\gamma_2},$$

and $\gamma < 1$.

Then we have the following Bernstein-type inequality.

Theorem A.3 (Theorem 1 in Merlevède et al. (2011)). *Under above assumptions, the constant V defined in (16) is finite. Moreover, for any $n \geq 4$, there exist positive constants C_1, C_2, C_3, C_4 , depending only on $a, b, c, \gamma_1, \gamma_2$, such that for all $x > 0$,*

$$\mathbb{P}\left(\max_{1 \leq j \leq n} |S_j| \geq x\right) \leq n \exp\left(-\frac{x^\gamma}{C_1}\right) + \exp\left(-\frac{x^2}{C_2(1+nV)}\right) + \exp\left(-\frac{x^2}{C_3n} \exp\left(\frac{x^{\gamma(1-\gamma)}}{C_4(\log x)^\gamma}\right)\right),$$

where $S_j = X_1 + X_2 + \dots + X_j$.

B. Distinction from Online Adaptation and Temporal Generalization Approaches

While TEFL enhances forecasting through error feedback, it differs fundamentally from methods that adapt models during deployment or explicitly model temporal distribution shifts. We briefly contrast our approach with two related paradigms.

First, *online adaptation* techniques update model parameters at inference time using newly observed data. A common design principle is to restrict updates to a small subset of parameters to maintain stability. For example, some works adjust only ensemble weights (Wen et al., 2023), adapter layers (Guo et al., 2024; Lee et al., 2025; Huang et al., 2025), or student network components (Lau et al., 2025). Full-model fine-tuning is generally avoided due to the risk of catastrophic forgetting or gradient instability when learning from single or few samples.

To mitigate noisy gradient estimates, several strategies have been proposed. Experience replay (Lau et al., 2025) incorporates historical observations into the loss computation, thereby reducing variance. Other approaches, such as FSNet (Pham et al., 2023), maintain dual pathways: one for rapid adaptation using recent data, and another for slow, stable updates based on accumulated experience. Notably, certain methods bypass backpropagation entirely; ELF (Lee et al., 2025), for instance, formulates the adapter as a linear regressor whose optimal solution can be computed analytically from a small batch of recent points.

Second, *temporal domain generalization (TDG)* seeks to improve robustness under continuously evolving data distributions by modeling the dynamics of domain change. Representative approaches include: Gradient Interpolation (GI) (Nasery et al., 2021), which enforces temporal smoothness in the loss landscape; LSSAE (Qin et al., 2022), which separates time-varying and invariant latent factors; and DRAIN (Bai et al., 2022), which uses a recurrent network to generate future model parameters. More recent work leverages dynamical systems theory—e.g., Koodos (Cai et al., 2024) and FreKoo (Yu et al., 2025) employ the Koopman operator to embed nonlinear temporal evolution into a linear predictive space, while STAD (Schirmer et al., 2024) treats classifier weights as drifting states governed by a state-space process.

In summary, both online adaptation and TDG require either parameter updates during inference or explicit modeling of how the data distribution evolves over time. In contrast, TEFL operates entirely offline: it treats past prediction

residuals—naturally available in rolling evaluation—as auxiliary inputs to a fixed model. No parameter modification, experience buffer, or temporal dynamics model is needed, making TEFL lightweight, universally compatible, and free of test-time computational overhead.

C. Datasets

The datasets used in the experiments are as follows.

The ETTm1 and ETTm2 (Liu et al., 2023) datasets contain the temperature and electric load data recorded every 15 minutes from transformers in two regions of China, covering the period from 2016 to 2018.

The Weather (Liu et al., 2023) dataset records 21 different meteorological indicators every 10 minutes across Germany for the year 2020. Key indicators include air temperature and visibility.

The Electricity dataset (Liu et al., 2023) contains the hourly electricity consumption records (in kW·h) of 321 clients. It is sourced from the UCL Machine Learning Repository and covers the period from 2012 to 2014.

The AQShunyi and AQWan datasets (Zhang et al., 2017; Qiu et al., 2024) record the hourly air quality in Beijing from 2013 to 2017, including 11 factors such as PM2.5 and PM10.

The ZafNoo and CzeLan datasets (Poyatos et al., 2020) record plant transpiration data every 30 minutes.

The EURUSD dataset records 6 indicators for the Euro/USD exchange rate, including the opening price, closing price, and trading volume, at 15-minute intervals from 2023 to 2024.

D. Experiment details

We provide the pseudo code for the training process of our method in Algorithm 1.

D.1. Hyperparameters

Regarding hyperparameters, for the base forecasting models, we adopt the hyperparameters from their official code repositories. For several datasets, such as AQShunyi, AQWAN, and EURUSD, the official codebases do not provide hyperparameters. Considering that these datasets are similar in size to the ETTm dataset, we use the hyperparameters corresponding to ETTm instead.

For our own method, the warm-up phase consists of three epochs. During the warm-up of the base model, the loss comprises two components: the base forecasting loss and the spectral flatness loss, with equal weights assigned to each. The training configurations, such as the learning rate, remain the same as those used for training the base model. During joint training, we train for 12 epochs with the AdamW optimizer. The remaining configurations, such as learning rate decay and patience, follow the default settings in official code repositories.

As for the error module, a bottleneck layer is first applied to reduce the error vector dimension; we set this dimension to 64.

D.2. Details of shock and distribution shift in the main te

Regarding Shock Injection: We uniformly injected 30 shocks across the entire dataset, ensuring consistent intervals between each shock. This ensures that shock events appear within the training, validation, and test sets. Shocks were applied to the normalized data. Each shock starts at its maximum amplitude of 3 and then linearly decays. The amplitude reaches zero at the 196th time step after the shock onset.

Regarding Distribution Shift: For the normalized dataset, let y_t represent the data at time step t , and L denote the total length of the dataset. We modified data points where $t > 0.5L$ as $y_t = y_t + \frac{4(t-0.5L)}{L}$. This introduces a linear drift, causing a gradually increasing distribution shift throughout the latter half of the data. All experiments under distribution are conducted without RevIN.

Algorithm 1 Training Procedure of TEFL

Require: Time series $\mathcal{D} = \{y_1, y_2, \dots, y_T\}$, horizon H , warm-up epochs E_w , total epochs E , regularization weight α

Ensure: Trained base model f and error module g

// Phase 1: Warm-up base model

```

1: for epoch = 1 to  $E_w$  do
2:   for each batch of samples  $\{(X_i, Y_i)\}_{i=1}^B$  from  $\mathcal{D}$  do
3:      $X_i = [y_{t-H}, \dots, y_{t-1}]$ ,  $Y_i = [y_t, \dots, y_{t+H-1}]$ 
4:      $\hat{Y}_i \leftarrow f(X_i)$ 
5:      $\epsilon_i \leftarrow Y_i - \hat{Y}_i$ 
6:      $\mathcal{L}_{\text{acc}} \leftarrow \frac{1}{B} \sum_{i=1}^B \|Y_i - \hat{Y}_i\|_1$ 
7:      $\mathcal{L}_{\text{sf}} \leftarrow \text{SF}(\epsilon_1, \dots, \epsilon_B)$ 
8:      $\mathcal{L} \leftarrow \mathcal{L}_{\text{acc}} + \alpha \cdot \mathcal{L}_{\text{sf}}$ 
9:     Update  $f$  via  $\nabla_f \mathcal{L}$ 
10:  end for
11: end for
    
```

// Phase 2: Joint training with causal error simulation

```

12: for epoch =  $E_w + 1$  to  $E$  do
13:   for each batch of samples constructed from contiguous segments of length  $3H$  do
14:     // Segment:  $[y_{t-2H}, \dots, y_{t+H-1}]$ 
15:      $X_{\text{ctx}} \leftarrow [y_{t-2H}, \dots, y_{t-H-1}]$  // context input
16:      $X_{\text{in}} \leftarrow [y_{t-H}, \dots, y_{t-1}]$  // current input
17:      $Y_{\text{hist}} \leftarrow [y_{t-H}, \dots, y_{t-1}]$  // true values for error
18:      $Y_{\text{tgt}} \leftarrow [y_t, \dots, y_{t+H-1}]$  // prediction target
19:      $\hat{Y}_{\text{ctx}} \leftarrow f(X_{\text{ctx}})$  // forecast for  $Y_{\text{hist}}$ 
20:      $\epsilon \leftarrow Y_{\text{hist}} - \hat{Y}_{\text{ctx}}$ 
21:      $\hat{Y}_{\text{base}} \leftarrow f(X_{\text{in}})$  // base forecast for  $Y_{\text{tgt}}$ 
22:      $\Delta \leftarrow g(\epsilon)$ 
23:      $\hat{Y}_{\text{final}} \leftarrow \hat{Y}_{\text{base}} + \Delta$ 
24:      $\mathcal{L} \leftarrow \mathcal{L}_{\text{acc}}(Y_{\text{tgt}}, \hat{Y}_{\text{final}})$ 
25:     Update both  $f$  and  $g$  via  $\nabla_{f,g} \mathcal{L}$ 
26:   end for
27: end for
    
```

D.3. Computational Overhead.

TEFL introduces modest computational and memory overhead during training, with negligible cost at inference. Specifically, in the joint training phase, each training sample is constructed from a contiguous segment of length $3H$, which is split into a context window and an input window. This requires doubling the batch size. Consequently, GPU memory consumption increases by a constant factor (typically less than $2 \times$), but this remains manageable on modern hardware.

Regarding training time, the only additional cost comes from the initial warm-up phase, which typically lasts for a small number of epochs (e.g., 3 in our experiments). The subsequent joint training phase has a per-epoch cost comparable to standard training. Thus, the total training time of TEFL is on the same order of magnitude as that of the standard training.

Critically, during deployment in rolling forecasting scenarios, TEFL incurs *negligible overhead*. The historical residuals $\epsilon_{t-H:t-1}$ are naturally available from previous predictions, and the lightweight error module g (e.g., a low-rank adapter) adds minimal latency. Therefore, TEFL offers its accuracy and robustness benefits with a highly favorable computation-accuracy trade-off.

E. Analysis of using longer input window

We also conducted experiments to investigate the effects of using longer input lengths on certain datasets. Specifically, for the ETTm1, ETTm2, and Weather datasets, we fixed the prediction horizon at 96 steps and sequentially extended the

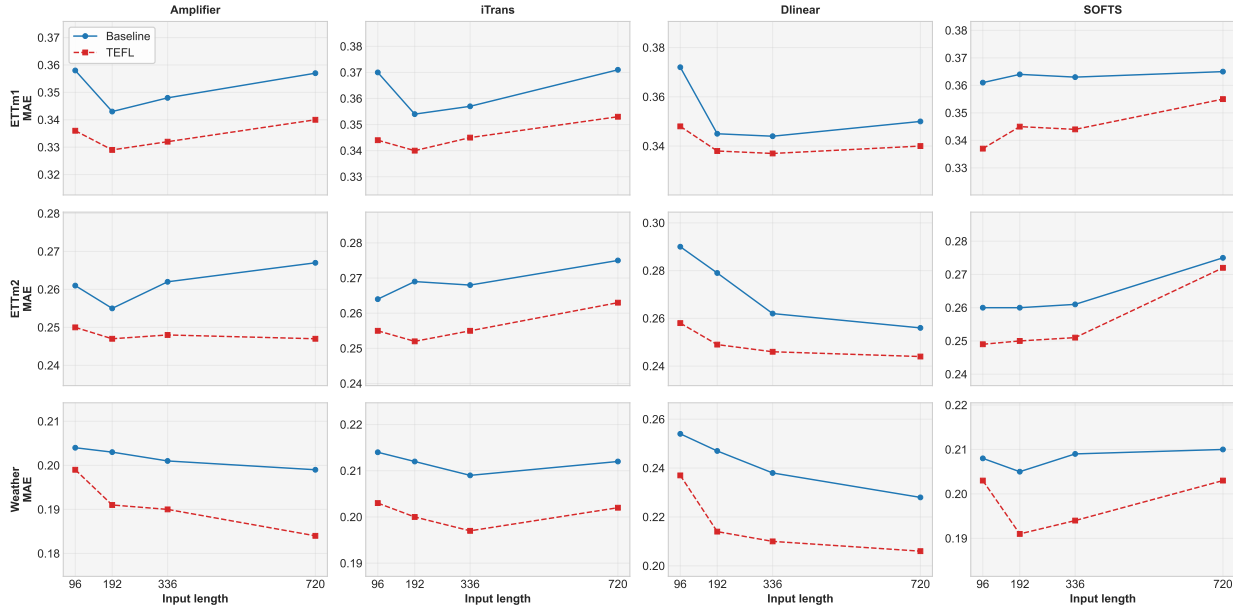


Figure 4. Comparison of Baseline and TEFL Methods for different input window size

look-back window length from 96 to 192, 336, and 720. We repeated the experiments under these configurations, training models with both the original method and our TEFL method. The resulting testset MAE for each setting is plotted in Figure 4.

First, a key finding is that regardless of the input window length, the accuracy achieved by TEFL method is consistently better than that of the original method. Second, for different datasets and models, there appears to be a different optimal input window length.

Finally, we would like to highlight that our method can utilize a longer historical context more effectively. For instance, when the input window size is 96, our method is somehow equivalent to extending the input size to 192 steps. This is because TEFL method first uses data from steps $t - 192$ to $t - 96$ to predict the segment from $t - 96$ to t . The error from this prediction is then incorporated, along with the original data from $t - 96$ to t , to generate the final forecast. The results of Figure 4 show that our method can be viewed as a more efficient way to integrate longer historical information. This is supported by comparing the second blue point (the original method with a 192-step lookback window) with the first red point (our method with a 96-step lookback window) in each subplot of Figure 4. The comparison shows that in most cases, directly extending the input window of the original model from 96 to 192 steps does not yield better results than using our method with a 96-step lookback window.

F. Discussion of training method

F.1. Discussion of spectral flatness

Spectral flatness is a commonly used metric to evaluate whether a time series possesses structure. If the spectral flatness is close to 1, it indicates that the time series has little structure and is close to white noise. Therefore, we introduce a regularization term using spectral flatness of the prediction errors at consecutive time steps. This ensures that the errors of the base model exhibit a certain structure over time, allowing the subsequent error module to learn more effectively.

To specifically illustrate the temporal patterns corresponding to different levels of spectral flatness, four time series examples are presented in Figure 5. Each row in the figure corresponds to one time series, arranged in descending order of spectral flatness from top to bottom. Each row contains two subplots: the left subplot displays the original time series, while the right subplot shows its frequency-domain energy distribution after Fourier transform.

From top to bottom, the spectral flatness of the time series decreases progressively. The top row represents white noise, which possesses the highest spectral flatness. In contrast, the bottom row corresponds to a pure sine wave, where nearly

all the energy is concentrated at a single frequency, resulting in a spectral flatness approaching zero. This visualization clearly demonstrates the close relationship between spectral flatness and the presence of temporal structure in a signal. Consequently, during pre-training, applying regularization to minimize the spectral flatness of prediction errors effectively preserves a certain degree of temporal structure within the error sequence.

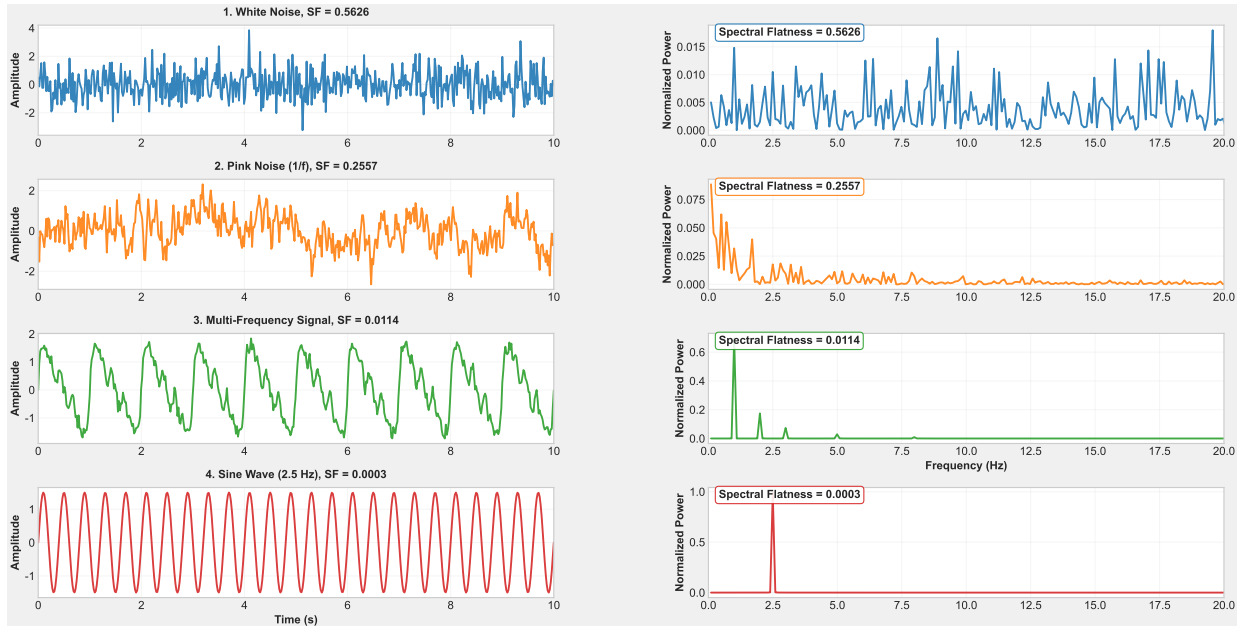


Figure 5. Examples about spectral flatness

F.2. Experiments using different training method

We conducted additional experiments on the ETTm and Weather datasets to compare different training schemes. Specifically, we considered the following three schemes: (1) first training the base forecasting model until convergence, then fixing the base model and training only the error module; (2) jointly training the base model and the error module from scratch; and (3) removing the spectral flatness regularization from our training method. The results of these training methods are presented in Table 4. In this table, the three schemes are labeled as Type 1, Type 2, and w/o SF (without spectral flatness). It can be observed that in most cases our method outperforms the other three variants. Moreover, Type 1 sometimes performs even worse than the original approach that does not incorporate error information. This may be because when the base model is trained to convergence, overfitting has already occurred, leading to a discrepancy of the error distributions between the training and test sets. Consequently, the error module trained solely on training set errors struggles to generalize to the test set. Meanwhile, the results of the w/o SF scheme also provide experimental evidence for the utility of the spectral flatness regularization term.

G. Discussion about historical errors

Figure 6 illustrates three choices of historical errors examined in this study, using the prediction of the next 96 steps as an example. The i -th row of each matrix represents the prediction errors for the next 96 steps at time i . The matrix displays the case at $t = 100$. Shaded areas represent unobservable errors, and red areas show the selected historical errors. The first subfigure corresponds to the error selection introduced in the main text. At time t , prediction errors for steps 1 to 96 ahead at time $t - 96$ are selected. The second subfigure uses the one-step-ahead prediction errors at times $t - 96, t - 95, \dots, t - 1$ as the input for error module. The third subfigure uses the prediction errors for time t at times $t - 96, t - 95, \dots, t - 1$.

Intuitively, the choice in subfigure 3 may appear more reasonable. This is because all error calculations use the true value at time t , i.e., the most recently observed data, thus minimizing latency. However, what are the actual results? Table 5 reports the experimental results for these three error selections. In the table, TEFL refers to the choice from the main text. Type2 and Type3 correspond to the error selections shown in the second and third subfigure, respectively.

TEFL: Temporal Error Feedback Learning

Table 4. Results of different training methods

Model	Metric	SOFTS		iTrans		Dlinear		TimeFilter		Amplifier		AVG		
		MSE	MAE											
ETTm1	96	Baseline	0.322	0.361	0.344	0.370	0.345	0.372	0.315	0.356	0.316	0.358	0.329	0.363
		Type 1	0.323	0.364	0.342	0.380	0.344	0.376	0.321	0.361	0.317	0.359	0.330	0.368
		Type 2	0.300	0.340	0.319	0.347	0.318	0.351	0.300	0.336	0.304	0.336	0.308	0.342
		w\o SF	0.321	0.363	0.333	0.370	0.341	0.374	0.324	0.364	0.320	0.361	0.328	0.366
		TEFL	0.299	0.337	0.314	0.344	0.311	0.348	0.299	0.336	0.298	0.336	0.304	0.340
	192	Baseline	0.376	0.390	0.380	0.394	0.382	0.391	0.359	0.381	0.365	0.384	0.372	0.388
		Type 1	0.390	0.400	0.367	0.391	0.359	0.384	0.351	0.377	0.348	0.376	0.363	0.386
		Type 2	0.345	0.364	0.358	0.375	0.351	0.370	0.345	0.362	0.346	0.361	0.349	0.366
		w\o SF	0.354	0.381	0.360	0.383	0.364	0.386	0.350	0.375	0.351	0.375	0.356	0.380
		TEFL	0.343	0.363	0.357	0.375	0.353	0.369	0.343	0.361	0.342	0.360	0.347	0.366
	336	Baseline	0.408	0.414	0.419	0.418	0.414	0.414	0.390	0.403	0.396	0.406	0.406	0.411
		Type 1	0.405	0.414	0.397	0.413	0.392	0.411	0.378	0.395	0.373	0.397	0.389	0.406
Type 2		0.382	0.391	0.386	0.394	0.382	0.394	0.374	0.384	0.377	0.384	0.380	0.389	
w\o SF		0.382	0.403	0.383	0.401	0.386	0.403	0.378	0.395	0.373	0.393	0.380	0.399	
TEFL		0.370	0.384	0.389	0.397	0.380	0.390	0.376	0.384	0.375	0.384	0.377	0.387	
720	Baseline	0.468	0.449	0.490	0.458	0.473	0.450	0.460	0.437	0.455	0.441	0.469	0.447	
	Type 1	0.461	0.450	0.465	0.453	0.447	0.446	0.452	0.433	0.444	0.439	0.454	0.444	
	Type 2	0.442	0.428	0.440	0.433	0.449	0.440	0.450	0.434	0.444	0.426	0.445	0.432	
	w\o SF	0.442	0.441	0.460	0.436	0.449	0.441	0.449	0.430	0.440	0.431	0.448	0.436	
	TEFL	0.437	0.426	0.459	0.434	0.442	0.428	0.445	0.423	0.449	0.433	0.445	0.429	
ETTm2	96	Baseline	0.180	0.260	0.181	0.264	0.193	0.290	0.171	0.258	0.178	0.261	0.181	0.267
		Type 1	0.178	0.259	0.182	0.267	0.194	0.288	0.173	0.261	0.176	0.257	0.181	0.266
		Type 2	0.172	0.250	0.172	0.252	0.173	0.253	0.170	0.254	0.174	0.255	0.172	0.253
		w\o SF	0.172	0.254	0.187	0.270	0.191	0.283	0.188	0.270	0.181	0.261	0.184	0.268
		TEFL	0.169	0.249	0.173	0.255	0.177	0.258	0.167	0.250	0.171	0.250	0.171	0.252
	192	Baseline	0.247	0.308	0.253	0.314	0.283	0.360	0.237	0.300	0.240	0.300	0.252	0.316
		Type 1	0.243	0.303	0.241	0.305	0.283	0.354	0.236	0.301	0.234	0.298	0.247	0.312
		Type 2	0.236	0.299	0.232	0.293	0.233	0.295	0.233	0.290	0.230	0.291	0.233	0.294
		w\o SF	0.237	0.298	0.241	0.305	0.259	0.332	0.240	0.304	0.237	0.301	0.243	0.308
		TEFL	0.235	0.298	0.239	0.300	0.238	0.300	0.231	0.292	0.233	0.293	0.235	0.296
	336	Baseline	0.312	0.348	0.311	0.351	0.372	0.421	0.294	0.336	0.301	0.340	0.318	0.359
		Type 1	0.291	0.338	0.292	0.341	0.371	0.414	0.290	0.331	0.287	0.336	0.306	0.352
Type 2		0.290	0.337	0.289	0.336	0.292	0.337	0.288	0.334	0.291	0.339	0.290	0.337	
w\o SF		0.283	0.330	0.290	0.339	0.324	0.377	0.289	0.338	0.294	0.336	0.296	0.344	
TEFL		0.290	0.335	0.292	0.339	0.295	0.342	0.281	0.329	0.289	0.334	0.287	0.335	
720	Baseline	0.476	0.404	0.412	0.406	0.535	0.513	0.392	0.397	0.396	0.397	0.442	0.423	
	Type 1	0.390	0.395	0.384	0.400	0.507	0.490	0.386	0.398	0.383	0.395	0.410	0.416	
	Type 2	0.387	0.396	0.398	0.404	0.414	0.424	0.383	0.399	0.386	0.392	0.394	0.403	
	w\o SF	0.387	0.397	0.398	0.404	0.453	0.456	0.388	0.397	0.384	0.392	0.402	0.409	
	TEFL	0.388	0.399	0.392	0.399	0.400	0.411	0.381	0.394	0.379	0.391	0.388	0.399	
Weather	96	Baseline	0.168	0.208	0.174	0.214	0.196	0.254	0.156	0.201	0.156	0.204	0.170	0.216
		Type 1	0.178	0.209	0.173	0.216	0.199	0.253	0.161	0.205	0.155	0.203	0.173	0.217
		Type 2	0.165	0.205	0.169	0.207	0.190	0.245	0.152	0.196	0.154	0.201	0.166	0.211
		w\o SF	0.183	0.222	0.193	0.228	0.196	0.239	0.175	0.218	0.170	0.215	0.183	0.224
		TEFL	0.166	0.203	0.167	0.203	0.195	0.237	0.155	0.198	0.153	0.199	0.166	0.208
	192	Baseline	0.220	0.256	0.225	0.258	0.237	0.297	0.204	0.249	0.210	0.250	0.219	0.262
		Type 1	0.222	0.260	0.220	0.251	0.234	0.289	0.205	0.248	0.213	0.257	0.219	0.261
		Type 2	0.219	0.250	0.218	0.250	0.225	0.287	0.201	0.243	0.208	0.245	0.214	0.255
		w\o SF	0.220	0.258	0.223	0.259	0.221	0.271	0.210	0.251	0.216	0.255	0.218	0.259
		TEFL	0.221	0.256	0.211	0.247	0.227	0.271	0.195	0.239	0.210	0.248	0.211	0.251
	336	Baseline	0.277	0.297	0.282	0.299	0.282	0.331	0.263	0.291	0.269	0.293	0.274	0.302
		Type 1	0.280	0.300	0.281	0.295	0.277	0.329	0.264	0.289	0.259	0.290	0.272	0.301
Type 2		0.268	0.296	0.265	0.289	0.259	0.321	0.249	0.283	0.253	0.290	0.259	0.296	
w\o SF		0.264	0.293	0.262	0.293	0.258	0.302	0.252	0.284	0.262	0.292	0.260	0.293	
TEFL		0.258	0.288	0.257	0.285	0.266	0.307	0.245	0.276	0.246	0.282	0.254	0.288	
720	Baseline	0.358	0.349	0.350	0.344	0.349	0.381	0.341	0.343	0.348	0.343	0.349	0.352	
	Type 1	0.357	0.349	0.348	0.341	0.350	0.379	0.344	0.346	0.340	0.339	0.348	0.351	
	Type 2	0.320	0.333	0.321	0.335	0.319	0.350	0.317	0.330	0.324	0.338	0.320	0.337	
	w\o SF	0.322	0.338	0.325	0.336	0.327	0.355	0.313	0.328	0.317	0.327	0.321	0.337	
	TEFL	0.319	0.327	0.321	0.329	0.324	0.352	0.312	0.324	0.315	0.326	0.318	0.331	

As shown in Table 5, our proposed TEFL method achieves the best performance in most cases. Only in a few long-term

forecasting tasks with prediction horizons of 336 and 720 steps does Type3 outperform TEFL.

We can analyze this phenomenon as follows. First, it is important to clarify that our method can be regarded as an approach using historical prediction errors to estimate the current prediction errors. However, all errors defined by Type2 are one-step-ahead prediction errors, whereas the current prediction errors are multi-step errors for the next 1 to 96 steps. The distributions of these two types of errors are clearly different, making it challenging to estimate multi-step errors solely based on one-step errors.

As for Type3, it performs better in a few long-term forecasting cases (e.g., 336 and 720 steps) because it indeed uses the most recently observed data, resulting in lower latency, which is advantageous for long-term predictions. However, its drawback lies in that all errors are calculated based on the true value at time t , leading to higher volatility (e.g., when there is an obvious outlier at time t). In contrast, TEFL incorporates true values from multiple time steps ($t, t - 1, \dots$), increasing the amount of information and reducing the impact of random fluctuations.

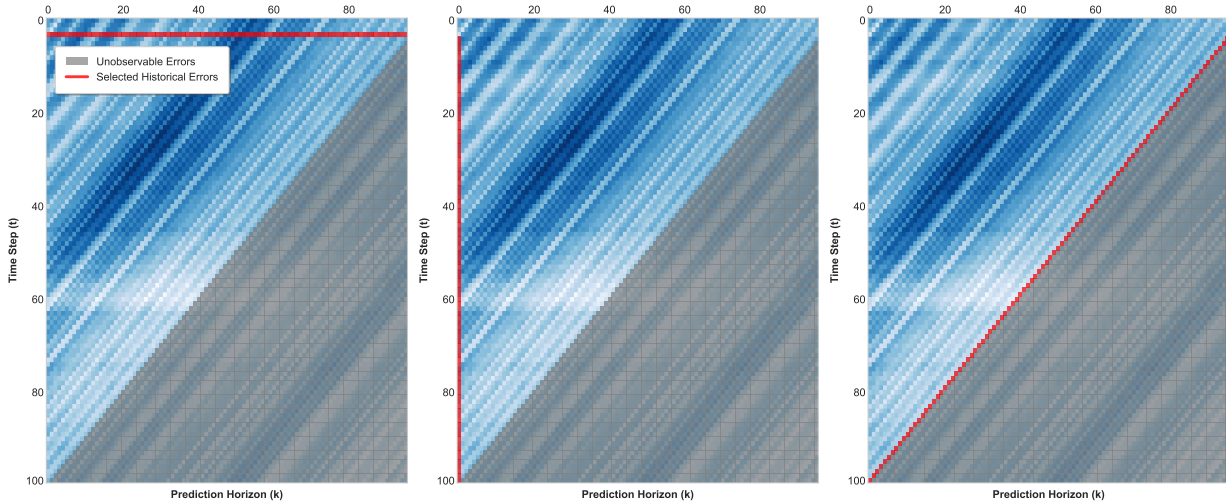


Figure 6. Different choices of historical errors

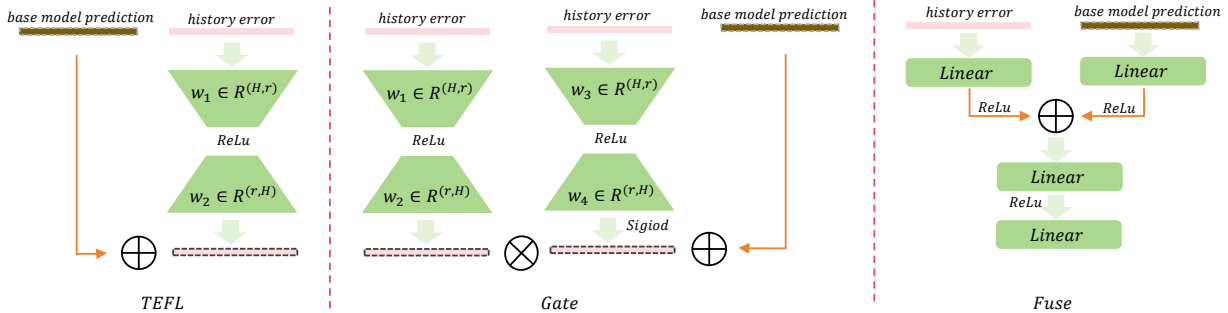


Figure 7. Different error modules

H. Discussion about error module

Figure 7 illustrates three different error module structures explored in this study. The first sub-figure corresponds to the structure adopted in the main text of the paper. The second and third sub-figures present two alternative designs. The second module design is called the "Gate" scheme, because, compared with the original error module of TEFL, it introduces a gating mechanism: the historical errors are passed through a feed-forward network (FFN), multiplied by a confidence score (generated by the another FFN), and then added to the base model's predictions. This design additionally considers the confidence of error correction; Intuitively, it should learn when to rely more on historical errors to correct the base model's predictions and when to trust the base model's predictions more. The design in the third sub-figure is called the "Fuse"

TEFL: Temporal Error Feedback Learning

Table 5. Results of different error selection methods

Model	Metric	SOFTS		iTrans		Dlinear		TimeFilter		Amplifier		AVG		
		MSE	MAE	MSE	MAE	MSE	MAE	MSE	MAE	MSE	MAE	MSE	MAE	
ETTm1	96	Baseline	0.322	0.361	0.344	0.370	0.345	0.372	0.315	0.356	0.316	0.358	0.329	0.363
		Type2	0.323	0.361	0.339	0.375	0.333	0.367	0.318	0.358	0.313	0.354	0.325	0.363
		Type3	0.323	0.363	0.340	0.378	0.334	0.369	0.318	0.358	0.312	0.354	0.325	0.364
		TEFL	0.299	0.337	0.314	0.344	0.311	0.348	0.299	0.336	0.298	0.336	0.304	0.340
	192	Baseline	0.376	0.390	0.380	0.394	0.382	0.391	0.359	0.381	0.365	0.384	0.372	0.388
		Type2	0.375	0.392	0.378	0.393	0.371	0.386	0.356	0.379	0.357	0.380	0.368	0.386
		Type3	0.387	0.400	0.362	0.388	0.356	0.381	0.348	0.377	0.352	0.378	0.361	0.385
		TEFL	0.343	0.363	0.357	0.375	0.353	0.369	0.343	0.361	0.342	0.360	0.348	0.366
	336	Baseline	0.408	0.414	0.419	0.418	0.414	0.414	0.390	0.403	0.396	0.406	0.406	0.411
		Type2	0.402	0.411	0.417	0.420	0.401	0.407	0.381	0.401	0.388	0.402	0.398	0.408
		Type3	0.408	0.416	0.397	0.413	0.385	0.405	0.372	0.399	0.378	0.400	0.388	0.407
		TEFL	0.370	0.384	0.389	0.397	0.380	0.390	0.376	0.384	0.375	0.384	0.378	0.388
720	Baseline	0.468	0.449	0.490	0.458	0.473	0.450	0.460	0.437	0.455	0.441	0.469	0.447	
	Type2	0.464	0.446	0.484	0.459	0.465	0.450	0.447	0.437	0.454	0.439	0.463	0.446	
	Type3	0.474	0.457	0.461	0.453	0.449	0.445	0.434	0.434	0.440	0.437	0.452	0.445	
	TEFL	0.437	0.426	0.459	0.434	0.442	0.428	0.445	0.423	0.449	0.433	0.446	0.429	
ETTm2	96	Baseline	0.180	0.260	0.181	0.264	0.193	0.290	0.171	0.258	0.178	0.261	0.181	0.267
		Type2	0.179	0.261	0.182	0.265	0.191	0.284	0.172	0.257	0.177	0.258	0.180	0.265
		Type3	0.181	0.262	0.181	0.265	0.191	0.284	0.173	0.257	0.177	0.258	0.181	0.265
		TEFL	0.169	0.249	0.173	0.255	0.177	0.258	0.167	0.250	0.171	0.250	0.171	0.252
	192	Baseline	0.247	0.308	0.253	0.314	0.283	0.360	0.237	0.300	0.240	0.300	0.252	0.316
		Type2	0.245	0.302	0.244	0.307	0.276	0.345	0.234	0.297	0.241	0.301	0.248	0.311
		Type3	0.236	0.298	0.241	0.304	0.272	0.340	0.230	0.296	0.235	0.297	0.243	0.307
		TEFL	0.235	0.298	0.239	0.300	0.238	0.300	0.231	0.292	0.233	0.293	0.235	0.296
	336	Baseline	0.312	0.348	0.311	0.351	0.372	0.421	0.294	0.336	0.301	0.340	0.318	0.359
		Type2	0.304	0.343	0.304	0.344	0.365	0.407	0.292	0.335	0.301	0.340	0.313	0.354
		Type3	0.289	0.335	0.291	0.339	0.344	0.393	0.282	0.330	0.283	0.332	0.298	0.346
		TEFL	0.290	0.335	0.292	0.339	0.295	0.342	0.281	0.329	0.289	0.334	0.289	0.336
720	Baseline	0.476	0.404	0.412	0.406	0.535	0.513	0.392	0.397	0.396	0.397	0.442	0.423	
	Type2	0.402	0.398	0.402	0.400	0.533	0.509	0.391	0.397	0.397	0.397	0.425	0.420	
	Type3	0.372	0.391	0.382	0.395	0.490	0.479	0.364	0.390	0.362	0.386	0.394	0.408	
	TEFL	0.388	0.399	0.392	0.399	0.400	0.411	0.381	0.394	0.379	0.391	0.388	0.399	
Weather	96	Baseline	0.168	0.208	0.174	0.214	0.196	0.254	0.156	0.201	0.156	0.204	0.170	0.216
		Type2	0.167	0.206	0.174	0.213	0.185	0.224	0.160	0.202	0.194	0.229	0.176	0.215
		Type3	0.166	0.206	0.175	0.217	0.181	0.227	0.158	0.202	0.190	0.226	0.174	0.216
		TEFL	0.166	0.203	0.167	0.203	0.195	0.237	0.155	0.198	0.153	0.199	0.167	0.208
	192	Baseline	0.220	0.256	0.225	0.258	0.237	0.297	0.204	0.249	0.210	0.250	0.219	0.262
		Type2	0.218	0.250	0.222	0.252	0.223	0.265	0.208	0.247	0.208	0.248	0.216	0.252
		Type3	0.209	0.248	0.214	0.254	0.218	0.268	0.200	0.244	0.201	0.244	0.208	0.252
		TEFL	0.221	0.256	0.211	0.247	0.227	0.271	0.195	0.239	0.210	0.248	0.213	0.252
	336	Baseline	0.277	0.297	0.282	0.299	0.282	0.331	0.263	0.291	0.269	0.293	0.274	0.302
		Type2	0.270	0.291	0.278	0.298	0.260	0.306	0.264	0.288	0.275	0.295	0.269	0.296
		Type3	0.257	0.286	0.258	0.289	0.267	0.301	0.248	0.281	0.258	0.287	0.258	0.289
		TEFL	0.258	0.288	0.257	0.285	0.266	0.307	0.245	0.276	0.246	0.282	0.254	0.288
720	Baseline	0.358	0.349	0.350	0.344	0.349	0.381	0.341	0.343	0.348	0.343	0.349	0.352	
	Type2	0.350	0.346	0.346	0.340	0.330	0.350	0.341	0.339	0.345	0.340	0.343	0.343	
	Type3	0.327	0.336	0.323	0.337	0.322	0.355	0.315	0.328	0.320	0.331	0.321	0.337	
	TEFL	0.319	0.327	0.321	0.329	0.324	0.352	0.312	0.324	0.315	0.326	0.318	0.331	

method. It projects both the errors and the base model predictions, merges them, and then passes the result through an FFN to obtain the final output, thereby allowing the interaction between historical errors and the base model predictions to be considered.

Table 6 reports the experimental results of these three schemes on the ETTm and Weather datasets. It can be observed that these two variants do not outperform the original, simplest TEFL method in most cases. Especially for the "Fuse" method, although it possesses strong expressive power in theory, it even performs worse than the baseline method without an error

module on the ETTm dataset, which may be caused by overfitting due to its excessive number of parameters.

Table 6. Results of different error modules

Model Metric		SOFTS		iTrans		Dlinear		TimeFilter		Amplifier		AVG		
		MSE	MAE	MSE	MAE	MSE	MAE	MSE	MAE	MSE	MAE	MSE	MAE	
ETTm1	96	Baseline	0.322	0.361	0.344	0.370	0.345	0.372	0.315	0.356	0.316	0.358	0.329	0.363
		Gate	0.320	0.345	0.320	0.349	0.328	0.349	0.310	0.337	0.326	0.350	0.321	0.346
		Fuse	0.377	0.408	0.411	0.425	0.412	0.426	0.410	0.428	0.367	0.402	0.395	0.418
		TEFL	0.299	0.337	0.314	0.344	0.311	0.348	0.299	0.336	0.298	0.336	0.304	0.340
	192	Baseline	0.376	0.390	0.380	0.394	0.382	0.391	0.359	0.381	0.365	0.384	0.372	0.388
		Gate	0.375	0.374	0.369	0.376	0.372	0.370	0.361	0.365	0.374	0.372	0.370	0.372
		Fuse	0.402	0.422	0.434	0.437	0.434	0.437	0.440	0.441	0.393	0.414	0.421	0.430
		TEFL	0.343	0.363	0.357	0.375	0.353	0.369	0.343	0.361	0.342	0.360	0.348	0.366
	336	Baseline	0.408	0.414	0.419	0.418	0.414	0.414	0.390	0.403	0.396	0.406	0.406	0.411
		Gate	0.416	0.401	0.404	0.397	0.403	0.392	0.393	0.386	0.407	0.394	0.405	0.394
		Fuse	0.427	0.439	0.455	0.453	0.453	0.450	0.464	0.456	0.420	0.435	0.444	0.446
		TEFL	0.370	0.384	0.389	0.397	0.380	0.390	0.376	0.384	0.375	0.384	0.378	0.388
	720	Baseline	0.468	0.449	0.490	0.458	0.473	0.450	0.460	0.437	0.455	0.441	0.469	0.447
		Gate	0.478	0.438	0.471	0.435	0.463	0.430	0.459	0.424	0.464	0.427	0.467	0.431
		Fuse	0.478	0.468	0.504	0.481	0.496	0.476	0.505	0.478	0.630	0.540	0.523	0.489
		TEFL	0.437	0.426	0.459	0.434	0.442	0.428	0.445	0.423	0.449	0.433	0.446	0.429
ETTm2	96	Baseline	0.180	0.260	0.181	0.264	0.193	0.290	0.171	0.258	0.178	0.261	0.181	0.267
		Gate	0.173	0.249	0.174	0.255	0.180	0.259	0.170	0.250	0.178	0.256	0.175	0.254
		Fuse	0.231	0.318	0.232	0.326	0.223	0.319	0.236	0.330	0.224	0.316	0.229	0.322
		TEFL	0.169	0.249	0.173	0.255	0.177	0.258	0.167	0.250	0.171	0.250	0.171	0.252
	192	Baseline	0.247	0.308	0.253	0.314	0.283	0.360	0.237	0.300	0.240	0.300	0.252	0.316
		Gate	0.240	0.300	0.239	0.297	0.240	0.298	0.231	0.292	0.242	0.299	0.238	0.297
		Fuse	0.292	0.357	0.292	0.360	0.298	0.365	0.297	0.364	0.294	0.362	0.295	0.361
		TEFL	0.235	0.298	0.239	0.300	0.238	0.300	0.231	0.292	0.233	0.293	0.235	0.296
	336	Baseline	0.312	0.348	0.311	0.351	0.372	0.421	0.294	0.336	0.301	0.340	0.318	0.359
		Gate	0.297	0.334	0.297	0.344	0.297	0.339	0.287	0.329	0.292	0.335	0.294	0.336
		Fuse	0.349	0.389	0.349	0.393	0.349	0.394	0.354	0.397	0.346	0.391	0.349	0.393
		TEFL	0.290	0.335	0.292	0.339	0.295	0.342	0.281	0.329	0.289	0.334	0.289	0.336
	720	Baseline	0.476	0.404	0.412	0.406	0.535	0.513	0.392	0.397	0.396	0.397	0.442	0.423
		Gate	0.400	0.400	0.391	0.396	0.404	0.412	0.385	0.395	0.383	0.390	0.393	0.398
		Fuse	0.446	0.450	0.456	0.454	0.450	0.452	0.474	0.465	0.461	0.457	0.457	0.456
		TEFL	0.388	0.399	0.392	0.399	0.400	0.411	0.381	0.394	0.379	0.391	0.388	0.399
Weather	96	Baseline	0.168	0.208	0.174	0.214	0.196	0.254	0.156	0.201	0.156	0.204	0.170	0.216
		Gate	0.166	0.198	0.178	0.213	0.205	0.233	0.156	0.193	0.175	0.214	0.176	0.210
		Fuse	0.171	0.227	0.177	0.234	0.174	0.230	0.166	0.221	0.166	0.221	0.171	0.227
		TEFL	0.166	0.203	0.167	0.203	0.195	0.237	0.155	0.198	0.153	0.199	0.167	0.208
	192	Baseline	0.220	0.256	0.225	0.258	0.237	0.297	0.204	0.249	0.210	0.250	0.219	0.262
		Gate	0.209	0.243	0.223	0.253	0.242	0.268	0.199	0.236	0.241	0.264	0.223	0.253
		Fuse	0.210	0.261	0.212	0.265	0.229	0.274	0.205	0.257	0.211	0.262	0.213	0.264
		TEFL	0.221	0.256	0.211	0.247	0.227	0.271	0.195	0.239	0.210	0.248	0.213	0.252
	336	Baseline	0.277	0.297	0.282	0.299	0.282	0.331	0.263	0.291	0.269	0.293	0.274	0.302
		Gate	0.264	0.283	0.273	0.291	0.282	0.304	0.252	0.277	0.270	0.290	0.268	0.289
		Fuse	0.265	0.295	0.254	0.298	0.265	0.298	0.250	0.293	0.252	0.296	0.257	0.296
		TEFL	0.258	0.288	0.257	0.285	0.266	0.307	0.245	0.276	0.246	0.282	0.254	0.288
	720	Baseline	0.358	0.349	0.350	0.344	0.349	0.381	0.341	0.343	0.348	0.343	0.349	0.352
		Gate	0.341	0.336	0.349	0.343	0.338	0.351	0.334	0.332	0.342	0.336	0.341	0.340
		Fuse	0.325	0.339	0.322	0.343	0.315	0.342	0.315	0.333	0.318	0.336	0.319	0.339
		TEFL	0.319	0.327	0.321	0.329	0.324	0.352	0.312	0.324	0.315	0.326	0.318	0.331

I. Reconciling Batch Training with Rolling Forecasting

As highlighted in the introduction, a fundamental mismatch exists between standard training protocols and real-world deployment: models are typically trained on randomly shuffled segments using batch optimization, whereas in practice they operate in a rolling fashion—making predictions step-by-step (or horizon-by-horizon) while sequentially observing ground

truth and accumulating prediction residuals.

One might question why we retain batch training in our method despite acknowledging this mismatch. The reason is pragmatic yet principled: completely abandoning batch training would sacrifice scalability, convergence stability, and compatibility with modern deep architectures. Instead, TEFL seeks to *bridge* the gap by *mimicking* the rolling feedback loop within a batch-compatible framework.

Specifically, during training, we construct each sample as a contiguous subsequence of length $3H$, where: the first H steps serve as the historical context, the next H steps are used to compute a "simulated" residual history (by applying the base model f to predict them from the prior H steps), and the final H steps constitute the true prediction target.

The error feedback module g then takes the simulated residuals from the middle segment as input to correct the base prediction for the last H steps. Crucially, this simulation is performed *within each sample independently*, without requiring cross-sample sequential dependencies. Thus, samples can be shuffled and processed in parallel, preserving the efficiency of batch training.

This design approximates the rolling scenario: just as a deployed system uses past errors to inform future forecasts, our training samples embed a short "look-back-and-correct" cycle internally. While it does not fully replicate the long-term error propagation seen in true rolling evaluation (where errors can build up over hundreds of steps), it provides sufficient signal for the model to learn how to interpret and utilize recent residuals—a capability that consistently leads to improved performance at test time, as shown in our experiments.

In essence, TEFL does not fully eliminate the train–test mismatch, but it *injects a causal, rolling-like signal into batch training*. This compromise enables both practical training efficiency and meaningful adaptation to recent prediction behavior. This gives us the best of both worlds: the speed and simplicity of batch training, plus the ability to adapt based on recent prediction behavior—something standard batch methods miss, and full online methods achieve only at much higher computational cost.

J. Full results

J.1. Full results of main experiments

Full results of main experiments are provided in Table 7 and 8.

J.2. Full results of datasets with shocks

The complete experimental results on the shock-injected datasets are reported in Table 9. It can be observed that our TEFL method achieves a significant performance improvement on the dataset with shocks. Furthermore, the extent of this improvement is greater than that observed on the original dataset, which demonstrates the robustness and superior adaptability of TEFL to shock events.

J.3. Full results for datasets with distribution

Regarding the dataset with distribution shift, the complete experimental results are provided in Table 10. From this table, it can be observed that our method achieves a significant improvement in prediction accuracy under distribution shift, demonstrating its strong adaptability to such conditions. This finding aligns with the conclusions presented in the main text.

Table 7. Full results I

Model	Metric		SOFTS		iTrans		Dlinear		TimeFilter		Amplifier		Avg		Imp	
			MSE	MAE	MSE	MAE	MSE	MAE	MSE	MAE	MSE	MAE	MSE	MAE	MSE	MAE
ETTm1	96	Baseline	0.322	0.361	0.344	0.370	0.345	0.372	0.315	0.356	0.316	0.358	0.329	0.363	7.4%	6.4%
		TEFL	0.299	0.337	0.314	0.344	0.311	0.348	0.299	0.336	0.298	0.336	0.304	0.340		
	192	Baseline	0.376	0.390	0.380	0.394	0.382	0.391	0.359	0.381	0.365	0.384	0.372	0.388	6.7%	5.7%
		TEFL	0.343	0.363	0.357	0.375	0.353	0.369	0.343	0.361	0.342	0.360	0.348	0.366		
	336	Baseline	0.408	0.414	0.419	0.418	0.414	0.414	0.390	0.403	0.396	0.406	0.406	0.411	6.8%	5.7%
		TEFL	0.370	0.384	0.389	0.397	0.380	0.390	0.376	0.384	0.375	0.384	0.378	0.388		
	720	Baseline	0.468	0.449	0.490	0.458	0.473	0.450	0.460	0.437	0.455	0.441	0.469	0.447	4.8%	4.1%
		TEFL	0.437	0.426	0.459	0.434	0.442	0.428	0.445	0.423	0.449	0.433	0.446	0.429		
ETTm2	96	Baseline	0.180	0.260	0.181	0.264	0.193	0.290	0.171	0.258	0.178	0.261	0.181	0.267	5.2%	5.3%
		TEFL	0.169	0.249	0.173	0.255	0.177	0.258	0.167	0.250	0.171	0.250	0.171	0.252		
	192	Baseline	0.247	0.308	0.253	0.314	0.283	0.360	0.237	0.300	0.240	0.300	0.252	0.316	6.6%	6.3%
		TEFL	0.235	0.298	0.239	0.300	0.238	0.300	0.231	0.292	0.233	0.293	0.235	0.296		
	336	Baseline	0.312	0.348	0.311	0.351	0.372	0.421	0.294	0.336	0.301	0.340	0.318	0.359	9.0%	6.6%
		TEFL	0.290	0.335	0.292	0.339	0.295	0.342	0.281	0.329	0.289	0.334	0.289	0.336		
	720	Baseline	0.476	0.404	0.412	0.406	0.535	0.513	0.392	0.397	0.396	0.397	0.442	0.423	12.2%	5.8%
		TEFL	0.388	0.399	0.392	0.399	0.400	0.411	0.381	0.394	0.379	0.391	0.388	0.399		
Weather	96	Baseline	0.168	0.208	0.174	0.214	0.196	0.254	0.156	0.201	0.156	0.204	0.170	0.216	1.7%	4.0%
		TEFL	0.166	0.203	0.167	0.203	0.195	0.237	0.155	0.198	0.153	0.199	0.167	0.208		
	192	Baseline	0.220	0.256	0.225	0.258	0.237	0.297	0.204	0.249	0.210	0.250	0.219	0.262	2.9%	3.7%
		TEFL	0.221	0.256	0.211	0.247	0.227	0.271	0.195	0.239	0.210	0.248	0.213	0.252		
	336	Baseline	0.277	0.297	0.282	0.299	0.282	0.331	0.263	0.291	0.269	0.293	0.274	0.302	7.3%	4.8%
		TEFL	0.258	0.288	0.257	0.285	0.266	0.307	0.245	0.276	0.246	0.282	0.254	0.288		
	720	Baseline	0.358	0.349	0.350	0.344	0.349	0.381	0.341	0.343	0.348	0.343	0.349	0.352	8.9%	5.8%
		TEFL	0.319	0.327	0.321	0.329	0.324	0.352	0.312	0.324	0.315	0.326	0.318	0.331		
Electricity	96	Baseline	0.144	0.235	0.149	0.240	0.210	0.302	0.135	0.233	0.148	0.246	0.157	0.251	3.9%	3.8%
		TEFL	0.144	0.232	0.143	0.232	0.186	0.272	0.136	0.231	0.146	0.240	0.151	0.242		
	192	Baseline	0.161	0.252	0.165	0.256	0.212	0.306	0.156	0.251	0.160	0.253	0.171	0.264	4.8%	7.5%
		TEFL	0.158	0.245	0.157	0.246	0.187	0.276	0.156	0.248	0.156	0.204	0.163	0.244		
	336	Baseline	0.177	0.269	0.179	0.272	0.223	0.319	0.164	0.264	0.175	0.270	0.184	0.279	4.5%	3.5%
		TEFL	0.174	0.264	0.170	0.261	0.199	0.291	0.163	0.261	0.170	0.268	0.175	0.269		
	720	Baseline	0.214	0.303	0.222	0.322	0.260	0.351	0.185	0.287	0.209	0.299	0.218	0.313	4.6%	4.3%
		TEFL	0.209	0.302	0.204	0.292	0.235	0.322	0.183	0.283	0.208	0.297	0.208	0.299		
EURUSD	96	Baseline	0.082	0.157	0.085	0.157	0.099	0.188	0.081	0.154	0.102	0.169	0.090	0.165	7.8%	4.9%
		TEFL	0.082	0.154	0.081	0.153	0.093	0.176	0.080	0.152	0.079	0.149	0.083	0.157		
	192	Baseline	0.112	0.201	0.115	0.202	0.133	0.230	0.109	0.196	0.110	0.196	0.116	0.205	2.6%	1.4%
		TEFL	0.111	0.199	0.109	0.197	0.129	0.225	0.108	0.196	0.107	0.193	0.113	0.202		
	336	Baseline	0.150	0.252	0.151	0.253	0.189	0.291	0.148	0.247	0.196	0.290	0.167	0.267	7.1%	4.2%
		TEFL	0.150	0.250	0.148	0.249	0.183	0.285	0.148	0.247	0.147	0.245	0.155	0.255		
	720	Baseline	0.270	0.356	0.279	0.362	0.366	0.427	0.274	0.353	0.275	0.358	0.293	0.371	1.3%	0.9%
		TEFL	0.269	0.354	0.267	0.353	0.362	0.423	0.272	0.352	0.274	0.357	0.289	0.368		

Table 8. Full results II

Model	Metric		SOFTS		iTrans		Dlinear		TimeFilter		Amplifier		Avg		Imp	
			MSE	MAE	MSE	MAE	MSE	MAE	MSE	MAE	MSE	MAE	MSE	MAE	MSE	MAE
AQWan	96	Baseline	0.814	0.489	0.832	0.498	0.784	0.512	0.803	0.486	0.788	0.483	0.804	0.494	2.4%	3.6%
		TEFL	0.782	0.476	0.800	0.478	0.783	0.484	0.788	0.475	0.770	0.465	0.785	0.476		
	192	Baseline	0.877	0.512	0.889	0.516	0.843	0.537	0.870	0.510	0.844	0.508	0.865	0.516	7.0%	5.0%
		TEFL	0.803	0.492	0.816	0.494	0.802	0.496	0.808	0.491	0.788	0.480	0.804	0.491		
	336	Baseline	0.891	0.522	0.907	0.527	0.856	0.546	0.884	0.519	0.872	0.523	0.882	0.527	6.4%	4.5%
		TEFL	0.823	0.505	0.839	0.508	0.822	0.509	0.828	0.504	0.815	0.494	0.826	0.504		
720	Baseline	0.949	0.545	0.960	0.547	0.909	0.570	0.954	0.547	0.923	0.542	0.939	0.550	5.0%	3.4%	
	TEFL	0.892	0.533	0.901	0.533	0.879	0.535	0.898	0.533	0.888	0.523	0.892	0.531			
ZafNoo	96	Baseline	0.471	0.410	0.474	0.417	0.454	0.433	0.478	0.418	0.517	0.436	0.479	0.423	3.3%	5.5%
		TEFL	0.462	0.392	0.467	0.401	0.446	0.400	0.477	0.410	0.462	0.394	0.463	0.400		
	192	Baseline	0.552	0.457	0.549	0.455	0.509	0.467	0.559	0.462	0.598	0.480	0.553	0.464	4.6%	4.8%
		TEFL	0.525	0.435	0.541	0.445	0.501	0.439	0.545	0.453	0.528	0.438	0.528	0.442		
	336	Baseline	0.607	0.487	0.595	0.481	0.540	0.484	0.614	0.491	0.749	0.608	0.621	0.510	8.4%	7.7%
		TEFL	0.570	0.466	0.580	0.471	0.535	0.470	0.587	0.480	0.573	0.467	0.569	0.471		
720	Baseline	0.708	0.535	0.690	0.527	0.576	0.505	0.720	0.543	1.011	0.766	0.741	0.575	16.1%	11.9%	
	TEFL	0.646	0.521	0.635	0.509	0.569	0.490	0.646	0.519	0.613	0.494	0.622	0.507			
Aqshunyi	96	Baseline	0.728	0.503	0.744	0.509	0.696	0.526	0.712	0.498	0.715	0.498	0.719	0.507	3.3%	4.3%
		TEFL	0.684	0.477	0.714	0.491	0.692	0.496	0.698	0.485	0.688	0.476	0.695	0.485		
	192	Baseline	0.779	0.522	0.790	0.527	0.743	0.547	0.765	0.518	0.740	0.515	0.764	0.526	6.9%	5.2%
		TEFL	0.702	0.492	0.733	0.506	0.706	0.505	0.716	0.500	0.698	0.490	0.711	0.498		
	336	Baseline	0.793	0.533	0.806	0.537	0.756	0.558	0.782	0.529	0.774	0.533	0.782	0.538	6.4%	4.9%
		TEFL	0.729	0.506	0.752	0.518	0.725	0.518	0.733	0.512	0.721	0.503	0.732	0.511		
720	Baseline	0.834	0.552	0.841	0.554	0.795	0.579	0.833	0.553	0.796	0.546	0.820	0.557	5.8%	4.3%	
	TEFL	0.768	0.526	0.782	0.535	0.763	0.540	0.779	0.537	0.770	0.526	0.772	0.533			
Solar	96	Baseline	0.201	0.236	0.207	0.238	0.287	0.375	0.193	0.223	0.222	0.284	0.222	0.271	10.7%	12.5%
		TEFL	0.183	0.248	0.200	0.222	0.223	0.230	0.183	0.209	0.202	0.278	0.198	0.237		
	192	Baseline	0.230	0.255	0.235	0.267	0.316	0.394	0.226	0.250	0.246	0.264	0.251	0.286	9.3%	14.0%
		TEFL	0.209	0.228	0.217	0.241	0.261	0.248	0.214	0.254	0.236	0.260	0.227	0.246		
	336	Baseline	0.248	0.270	0.250	0.278	0.349	0.412	0.234	0.261	0.271	0.297	0.271	0.304	13.4%	14.5%
		TEFL	0.213	0.275	0.232	0.254	0.265	0.250	0.218	0.270	0.244	0.250	0.234	0.260		
720	Baseline	0.246	0.272	0.250	0.281	0.354	0.410	0.239	0.268	0.272	0.297	0.272	0.306	13.9%	13.3%	
	TEFL	0.216	0.276	0.222	0.268	0.263	0.250	0.228	0.271	0.244	0.259	0.235	0.265			
CzeLan	96	Baseline	0.206	0.252	0.208	0.257	0.354	0.423	0.215	0.264	0.200	0.249	0.236	0.289	14.1%	16.0%
		TEFL	0.194	0.228	0.202	0.236	0.215	0.268	0.210	0.247	0.194	0.233	0.203	0.242		
	192	Baseline	0.237	0.271	0.240	0.280	0.471	0.476	0.245	0.283	0.235	0.274	0.285	0.317	18.5%	15.4%
		TEFL	0.222	0.254	0.232	0.260	0.250	0.301	0.238	0.268	0.222	0.257	0.233	0.268		
	336	Baseline	0.268	0.295	0.274	0.307	0.596	0.527	0.274	0.304	0.272	0.303	0.337	0.347	19.9%	13.0%
		TEFL	0.256	0.287	0.264	0.289	0.307	0.347	0.268	0.297	0.255	0.290	0.270	0.302		
720	Baseline	0.328	0.338	0.332	0.348	0.796	0.603	0.339	0.350	0.325	0.339	0.424	0.396	18.6%	9.0%	
	TEFL	0.326	0.343	0.323	0.339	0.447	0.440	0.319	0.342	0.310	0.336	0.345	0.360			

Table 9. Full results for dataset with shocks

Model	Metric	Amplifier	iTrans		Dlinear		SOFTS		TimeFilter		Avg		Imp			
			MSE	MAE	MSE	MAE	MSE	MAE	MSE	MAE	MSE	MAE	MSE	MAE		
ETTm1	96	Baseline	0.543	0.463	0.653	0.514	0.583	0.490	0.531	0.453	0.497	0.432	0.561	0.470	9.9%	8.9%
		TEFL	0.498	0.428	0.573	0.465	0.523	0.442	0.475	0.408	0.459	0.397	0.506	0.428		
	192	Baseline	0.541	0.459	0.657	0.512	0.686	0.543	0.648	0.511	0.600	0.487	0.626	0.503	10.1%	8.5%
		TEFL	0.490	0.423	0.589	0.472	0.594	0.478	0.594	0.478	0.548	0.447	0.563	0.460		
	336	Baseline	0.706	0.544	0.709	0.542	0.743	0.579	0.715	0.543	0.648	0.520	0.704	0.546	9.5%	7.9%
		TEFL	0.632	0.498	0.641	0.504	0.646	0.510	0.660	0.520	0.605	0.481	0.637	0.503		
	720	Baseline	0.810	0.598	0.798	0.588	0.832	0.629	0.811	0.598	0.754	0.573	0.801	0.597	9.7%	7.4%
		TEFL	0.698	0.546	0.733	0.552	0.747	0.568	0.742	0.566	0.695	0.531	0.723	0.553		
ETTm2	96	Baseline	0.340	0.335	0.326	0.334	0.414	0.430	0.317	0.325	0.315	0.322	0.342	0.349	8.3%	9.1%
		TEFL	0.318	0.316	0.311	0.316	0.336	0.343	0.303	0.305	0.302	0.306	0.314	0.317		
	192	Baseline	0.492	0.417	0.457	0.407	0.639	0.554	0.460	0.404	0.455	0.400	0.501	0.436	12.1%	11.0%
		TEFL	0.455	0.394	0.432	0.383	0.460	0.413	0.427	0.375	0.428	0.375	0.440	0.388		
	336	Baseline	0.643	0.493	0.559	0.463	0.823	0.650	0.557	0.457	0.554	0.457	0.627	0.504	15.6%	12.0%
		TEFL	0.556	0.455	0.520	0.435	0.550	0.474	0.510	0.423	0.512	0.428	0.530	0.443		
	720	Baseline	0.777	0.560	0.701	0.537	1.058	0.757	0.692	0.530	0.707	0.536	0.787	0.584	14.7%	9.5%
		TEFL	0.691	0.535	0.657	0.516	0.698	0.568	0.643	0.503	0.667	0.520	0.671	0.528		
Weather	96	Baseline	0.414	0.334	0.375	0.307	0.449	0.410	0.368	0.299	0.353	0.295	0.392	0.329	5.6%	10.4%
		TEFL	0.380	0.307	0.354	0.279	0.432	0.348	0.348	0.272	0.335	0.267	0.370	0.295		
	192	Baseline	0.568	0.423	0.502	0.386	0.584	0.506	0.500	0.387	0.476	0.375	0.526	0.415	7.7%	11.1%
		TEFL	0.508	0.384	0.483	0.365	0.516	0.403	0.466	0.350	0.456	0.345	0.486	0.369		
	336	Baseline	0.687	0.484	0.609	0.447	0.682	0.568	0.608	0.448	0.583	0.438	0.634	0.477	8.8%	10.2%
		TEFL	0.600	0.440	0.581	0.426	0.590	0.453	0.556	0.408	0.563	0.417	0.578	0.429		
	720	Baseline	0.815	0.555	0.709	0.506	0.761	0.625	0.702	0.503	0.674	0.493	0.732	0.536	11.1%	10.7%
		TEFL	0.668	0.486	0.669	0.484	0.659	0.511	0.633	0.459	0.626	0.456	0.651	0.479		

Table 10. Full results for datasets with distribution shift

Model	Metric	Amplifier		iTrans		Dlinear		SOFTS		TimeFilter		Avg		Imp		
		MSE	MAE	MSE	MAE	MSE	MAE	MSE	MAE	MSE	MAE	MSE	MAE	MSE	MAE	
ETTm1	96	Baseline	0.409	0.422	0.456	0.458	0.421	0.453	0.513	0.497	0.535	0.527	0.467	0.471	11.2%	10.2%
		TEFL	0.368	0.394	0.441	0.448	0.327	0.358	0.425	0.436	0.512	0.481	0.414	0.423		
	192	Baseline	0.424	0.428	0.493	0.482	0.496	0.505	0.483	0.477	0.558	0.547	0.491	0.488	12.6%	11.0%
		TEFL	0.392	0.401	0.429	0.443	0.393	0.409	0.454	0.452	0.475	0.466	0.429	0.434		
	336	Baseline	0.477	0.466	0.519	0.500	0.598	0.578	0.573	0.532	0.788	0.684	0.591	0.552	19.9%	15.2%
		TEFL	0.438	0.434	0.476	0.476	0.441	0.447	0.473	0.471	0.537	0.512	0.473	0.468		
	720	Baseline	0.579	0.519	0.657	0.594	0.840	0.724	0.768	0.650	0.765	0.654	0.722	0.628	18.8%	14.5%
		TEFL	0.544	0.486	0.624	0.574	0.572	0.538	0.581	0.535	0.610	0.551	0.586	0.537		
ETTm2	96	Baseline	0.193	0.292	0.186	0.287	0.194	0.299	0.192	0.295	0.200	0.302	0.193	0.295	7.2%	8.6%
		TEFL	0.181	0.268	0.178	0.271	0.176	0.263	0.185	0.283	0.176	0.265	0.179	0.270		
	192	Baseline	0.259	0.343	0.253	0.340	0.293	0.387	0.274	0.363	0.309	0.375	0.278	0.362	12.3%	12.0%
		TEFL	0.248	0.311	0.234	0.315	0.237	0.307	0.257	0.340	0.242	0.319	0.243	0.318		
	336	Baseline	0.347	0.409	0.330	0.400	0.378	0.451	0.404	0.451	0.425	0.455	0.377	0.433	21.3%	17.3%
		TEFL	0.298	0.353	0.286	0.352	0.294	0.349	0.304	0.370	0.302	0.367	0.297	0.358		
	720	Baseline	0.569	0.523	0.472	0.511	0.566	0.576	0.800	0.628	0.558	0.516	0.593	0.551	32.3%	20.6%
		TEFL	0.406	0.429	0.396	0.438	0.399	0.429	0.417	0.466	0.389	0.426	0.401	0.438		
Weather	96	Baseline	0.281	0.351	0.232	0.291	0.357	0.443	0.239	0.301	0.253	0.326	0.273	0.342	18.4%	16.3%
		TEFL	0.219	0.296	0.206	0.262	0.217	0.271	0.246	0.308	0.224	0.296	0.222	0.287		
	192	Baseline	0.362	0.412	0.329	0.367	0.479	0.522	0.417	0.435	0.322	0.388	0.382	0.425	21.6%	17.5%
		TEFL	0.237	0.291	0.328	0.382	0.254	0.305	0.397	0.429	0.282	0.346	0.299	0.351		
	336	Baseline	0.402	0.438	0.574	0.532	0.604	0.602	0.587	0.532	0.404	0.441	0.514	0.509	28.4%	21.6%
		TEFL	0.286	0.323	0.460	0.469	0.313	0.362	0.418	0.433	0.365	0.409	0.368	0.399		
	720	Baseline	0.717	0.601	0.666	0.582	0.807	0.717	0.552	0.517	0.578	0.555	0.664	0.594	29.2%	20.9%
		TEFL	0.400	0.420	0.476	0.468	0.446	0.467	0.572	0.520	0.458	0.475	0.470	0.470		